RSC Advances

ROYAL SOCIETY OF CHEMISTRY

www.rsc.org/advances

Graphene's Potential in Materials Science and Engineering

Xiang Zhang,[1*] Bhavatharini R. S. Rajaraman,[1] Huihui Liu [2] and Seeram Ramakrishna[1 *]

[1] Centre of Nanofibers & Nanotechnology, Department of Mechanical Engineering, Faculty of Engineering, National University of Singapore, 10 Kent Ridge Crescent, Singapore 117576

[2] Department of Medicine, Yong Loo Lin School of Medicine, National University of Singapore, 10 Kent Ridge Crescent, Singapore 119260

Corresponding Author
*E-mail: seeram@nus.edu.sg (S.R.).

ABSTRACT: Materials have become an indispensable part of our modern life, which was tailored such as good mechanical, electrical, thermal properties, etc. establish the basis and fundamentals and the governing rules for every modern technology. Things that were considered impossible have been made possible through the integrated approach of “needs driven” and “discovery driven” researches. One such approach resulted in a breakthrough in the discovery of Graphene, which was considered to be practically impossible. Graphene is the simplest and the strongest material ever found. Having demonstrated its potential in multifarious fields, graphene has consolidated itself as an invaluable material that can enhance or overhaul the existing paradigm in so many applications. This work is a consolidated review about exotic properties, various fabrication approaches, characterization techniques and promising applications of Graphene.

1. INTRODUCTION

The term "Graphene", which takes its roots from "Graphite" and "Alkene", was first coined to describe the single 2D sheets of graphite, as one of the constituents of Graphite Intercalation Compounds[1]. According to the formalized definition of IUPAC, graphene can be defined as a single carbon layer of the graphite structure, the nature of which can be described analogous to a polycyclic aromatic hydrocarbon of quasi infinite size and the term should be used only when the reactions, structural relations or other properties of individual layers are discussed[2]. Simply put in a layman's words, it is a thin, two dimensional, sheet of sp^2-bonded carbon, just an atom thick, densely packed into a hexagonal benzene-ringed structure, which makes it the building block for carbon based structures of all other dimensionalities.

The monolayer graphene is composed exclusively of six membered rings. But with the structural defects, it has five or seven membered rings or the combination of both, which makes it appear skewed or bent from its flat surface. The difference between the two defects is that the pentagonal defect occupies lesser space and causes the structure to roll into a cone whereas the heptagonal conformation needs more space and yields a saddle-like distortion. And a combination of these results in the formation of fullerene[3]. It can be righteously called as the mother of all other graphitic forms since it can be stacked one over the other to make 3D Graphite, or rolled into sheets of 2D carbon nanotubes, or wrapped up to form 0D Fullerenes (Buckyballs or cage molecules) and this has been shown in Fig 1.

2. EXOTIC PROPERTIES

Graphene is the first truly available two-dimensional material stable at room temperature, a feat long thought to be impossible[4-7] because of the thermal fluctuations in low dimensional crystal lattices that result in displacement of atoms, such that they become comparable to the interatomic distances at any finite temperature. The stability of the monolayer graphene can be attributed to the ripples[8] or corrugations observed at the microscopic level. These imperfections prevent the surface to get rolled

into tubes, owing to the thermodynamic stability[9] and also to suppress thermal vibrations[8] which offers stability for the planar dimensioned material. Graphene is also transparent, chemically inert and crystalline under ambient conditions. It is stronger and stiffer than diamond, but still as flexible as rubber, stretched by a quarter of its length. It has the largest known surface area to weight ratio. The strongest bond in nature, the C-C bond covalently locks these atoms in place, giving them remarkable mechanical properties[8, 10, 11].

2.1 Dirac Fermions

Normally, the electronic properties of materials are described by the Schrödinger equation. But the charge carriers in graphene strongly resemble the relativistic particles. Also, the interaction between the electrons and the 2D Honeycomb lattice of the graphene makes the electrons moving in it to behave as if they are massless. Because of this interaction and the symmetric nature of the honeycomb lattice, the electrons are governed by a more easier model that uses nearest neighbour, tight binding approach - Dirac's equation[12] for describing relativistic fermions (with spin, s= ½). However the speed of light that is used in this equation is replaced by the Fermi velocity, which is nearly 10^{-6} m/s. Hence the solution of Dirac equation gives a linear dispersion relation for the fermions. As a result, we can deduce that the fermions could be considered as massless particles (zero effective mass) inside the Graphene.

2.2 Berry's Phase

The linear low energy dispersion equation can be given by a spinor wave function, $\hat{H} = \hbar v_F \sigma k$, where σ is the pseudo-spin indicating the sub lattices A and B, which is parallel to the momentum of electrons and anti-parallel for holes. The projection of the pseudo-spin onto the direction of motion gives rise to a new internal degree of freedom, known as chirality. The origin of chirality can also be explained based on the Berry Phase concept. When a quasiparticle (electron or hole) encircles a closed contour in the momentum space, the wave function of a quasiparticle gains a phase shift known as "Berry's Phase". This phase shift occurs due to the rotation of pseudo-spin, when a quasiparticle repetitively moves between various carbon sub lattices (A and B for Single Layer Graphene; A1 and B2 for Bi-Layer Graphene and so on).

2.3 Zero Effective Mass

The model as presented in Fig 2 gives a Dirac cone-like spectrum of quasiparticles.[13] This peculiar electronic structure is what accounts for the unique properties of Graphene. The Fermi surface of Graphene is characterized by six *double cones*. In undoped graphene, the Fermi level is located at the points connecting the valence and conduction bands. At the Fermi level, the density of state is zero. In other words, no states can be occupied at that corresponding level, which means the electrical conductivity is pretty low. However the conductivity can be improved by changing the Fermi level using an electric field in such a way that the graphene becomes n-doped (with electrons) or p-doped (with holes) depending on the nature of polarity of the applied field. The electron dispersion relation becomes linear and the electrons behave as though zero effective mass. Hence the electrical conductivity is unparalleled at even room temperatures (greater than silver, the least resistive metallic material). Moreover, bi-layer graphene has a tuneable band gap and hence by using an electric field, it can be changed from conductor to semi-conductor.

2.4 Quantum Hall Effect

Hall Effect arises when a magnetic field is applied perpendicular to an electric field leading to the charges experiencing magnetic Lorentz force and accumulation at one end of the conductor. An asymmetric distribution of charge carriers over the surface occurred because of the equally opposite charged materials deflection to the opposite side. This separation between the charges establishes yet another electric field that prevents further charge to build up. As long as charges flow, there exists a steady electric potential, the Hall voltage and the magnetic field strength determines the resistivity of the conductor. The Quantum Hall Effect is a quantum phenomenon of the Hall Effect occurring on a macroscopic scale. It is exclusive to two dimensional materials with quantized values of conductivity and has elucidated various key aspects of quantum physics. The limitation is that it can be observed only at large magnetic field and very low temperatures (nearly 1K). Fortunately, graphene exhibits this phenomenon even at room temperature. (Bi-layer graphene agrees with the standard Hall Effect and

exhibits integer Hall effect, whereas the single layer graphene has a shift of ½ and falls under the Fractional Hall effect.

The valence and conductance band of graphene meets at the Dirac point (Fig 3. (b)), whereas that of conventional materials has a considerable band gap (Fig 3. (a)). Also, the recent ARPES studies of undoped graphene have demonstrated that there is an inward curvature (Fig 3. (c)), indicating electronic interactions occurring at increasingly longer range and leading to greater electron velocities. This electronic structure of graphene not only bridges the gap between valence band and the conduction band, but also, the gap between condensed matter physics and quantum electrodynamics.

2.5 Zitterbewegung

The electrons move effectively close to nearly 300 times lesser than the speed of light in vacuum allowing their relativistic effects to be observed without the use of particle accelerators. For instance, in Quantum Electro Dynamics (QED), the Zitterbewegung (the oscillatory motions – helical or circular – of the relativistic particles) arises due to the interference between particle and anti-particle states (positive and negative energy states). This interference produces an effect of fluctuation of the position of electrons at the speed of light. Generally this oscillatory motion is too fast to be spotted. But in graphene, the Compton wavelength of the Dirac Fermions which is of the order of one nanometer enables us to see this effect under high resolution microscope.

By classical physics, the rapid motion of the relativistic particles can also be attributed to the behaviour of an electron in presence of a potential created due to the presence of disorders in a crystal. The oscillating nature is the reason for the conductivity at zero temperature and zero chemical potential, in other words, the Zitterbewegung is similar to the intrinsic defects which cause a non-zero minimal conductivity in crystals without defects. This motion is also responsible for the particle spin and magnetic moment.

2.6 Klein Paradox

Another peculiar property of graphene is that, it exhibits the "Klein Paradox" effect whereby the relativistic electrons are able to pass through very large potential barrier. Also, the transmission of the

quantum particles through the barrier is sensitive to the barrier height. If the barrier heights are different for various spin orientations (magnetic gates), one can produce spin-polarized effects which allows one to manipulate the electron spin (Fig 4). This tunnelling effect has opened a possibility to study about the exotic but normally inaccessible relativistic, QED effects. For instance, this unimpeded penetration of relativistic particles through high, wide barriers predicts the pair production phenomenon which would normally require super-heavy nuclei or black holes.

2.7 Atomic Structure

Graphene consists of sp^2-bonded hybridised carbon atoms consisting of one "s" orbital and two "p" orbitals with bond length of 1.42 angstroms. This type of hybridisation makes it possess a trigonal planar structure. The s, p_x, p_y orbitals form σ - bonds with the nearest neighbouring carbon atoms. In general, the σ – bonds are the ones that determine the strength of a lattice structure, which is robust. Since the σ bands in graphene are completely filled, they form a deep valence band. But the p_z state is perpendicular to the planar structure and it laterally overlaps with the orbitals of neighbouring carbon atoms, resulting in a π - bond. Since each p-orbital has an excess electron, the band hence formed is half-filled.

2.8 Other Peculiar Behaviours

The basic properties of graphene are summarized in Table 1. In terms of high mobility semiconductors, graphene ranks the highest with a mobility of about 200,000 $cm^2 V^{-1} s^{-1}$, compared to silicon with 1,400 $cm^2 V^{-1} s^{-1}$ and Indium antimonide with 77,000 $cm^2 V^{-1} s^{-1}$, the highest mobility conventional semiconductor known ever. The very high mobility facilitates graphene to be employed in the transistors, chemical and bio-chemical sensing applications[14]. It can carry huge current densities up to 10^8 A cm^{-2}. Being a stable semi metal with a tiny overlap between valence and conductance bands under ambient conditions, they exhibit strong ambipolar electric field effect[15], allowing the control of both positive and negative charge carriers with concentrations equivalent to 10^{13} cm^{-2}. It is quite interesting that the composites when reinforced with graphene, perform better in terms of strength, stiffness and

failure resistance when compared to other nano-materials like carbon nanotubes, which might be a key to next era of nano-composite materials[16-18].

3. FABRICATION METHODS AND APPROACHES:

3.1 Conventional Approaches

To understand the trajectory of the research undergone in Graphene, it is a pre-requisite to know about the Graphite oxide (GO), Graphene Intercalation Compounds (GIC) and Graphene Oxide (RGO) since the Graphene has been synthesised by manipulating either of these materials. GIC's are formed by the insertion of atomic or molecular layers of a different chemical species called the intercalant between layers in a graphite host material. Graphite oxide is obtained by the strong oxidation of graphite with compounds like carbon, oxygen and hydrogen in variable ratios or by exfoliation of graphite powders. Graphene Oxide is a monolayer of the Graphite Oxide, usually obtained by exfoliating Graphite Oxide (GO).

Since time immemorial, preparation of the mono layer graphite has been a holy grail of Material Science. The quest for the wonder material dates back to the early 19th century, when a network of interwoven graphite layers with the intercalants was reported to be present in the GIC's and a scope for widening the interlaminar spacing was discovered[19]. On the verge of finding the structure of graphite, the research was taken to the next phase with the crystalline lamellar structure of graphite being brought to the limelight and confirmed using the X-Ray spectra. A distinct line of demarcation was drawn between the graphite and amorphous carbon by concluding that the former varies from the latter by its greater degree of sub-divisions, the lamellae, and the experiments were brought in the context of the chemical oxidation results[20].

By making chemical modifications in the previous researches, the successive researches were able to produce not only the intercalation compounds (GIC's)[21-23] but also, Graphite Oxide[24] by the chemical oxidation. However, these were just the stepping stones for the delamination of the graphite to its integral layers.

Then, another group was able to make freely suspended platelets of reduced Graphene oxide. The extremely fine lamellar carbon, so produced was obtained by either the deflagration of graphite oxide on heating, or reduction of Graphite Oxide in alkaline suspension[25]. The presence of monolayer graphite, otherwise called graphene, was confirmed by the LEED ring patterns developed while heating Platinum in Ultra-high vacuum[26, 27].

Further advancements were carried out on the analysis of the Graphene growth over the metals through the investigations of the surface coverage of carbon over temperature. These observations rendered a common conclusion that while heating to higher temperatures, the carbon dissolved in the metal alloys tends to undergo a phase separation as single and multiple layers of carbon over the metal surfaces, which confirmed the previous renditions by LEED and Auger electron Spectroscopy[28-30].

Then, experimentations were carried out on epitaxial growth of silicon by sublimation of an insulating substrate SiC and a monolayer of carbon, graphene was obtained by the electrical isolation. It was consolidated through the LEED and Auger spectroscopy, and the work featured an already proposed graphitisation mechanism of Badami[31, 32]. Similarly, numerous works have been carried out in the field of isolation of atomically thin graphene films over materials like Lanthanum Hexaboride (LaB_6)[33], Nickel[34], Iridium[35], Rhenium[36], Platinum[37], Tantalum carbide[38], Titanium carbide[39] and so on.

Pushing these chemical approaches aside, a unique yet simpler micromechanical approach was put forth to tailor the Highly Oriented Pyrolytic Graphite (HOPG) into uniformly spaced, small graphite islands, which was again an effort towards creating thin layers of graphite[40]. Meanwhile, there was an exclusive review encompassing the prediction and conception of graphene. But then, the multiple lamellae were not completely exfoliated into the corresponding monolayers of graphene previously. This approach was further honed and the task of obtaining pristine graphene layers was successfully accomplished by the following works[15, 41-43]. In spite of all these approaches, preparing large area, defect-free graphene of say, even a few squares of centimetres that can get a meaning for all these accomplishments and can be used for the commercial applications, remains the biggest challenge for the scientists.

Though the invention of pencil shed light to the presence of stacked layers of graphene building graphite, that are weakly coupled by van der Waals forces, it took nearly 440 years to isolate and *spot* it. The major reason was, it was believed that a material cannot exist stable in its two dimensional form. Also, they were not able to pinpoint how many layer the graphene sample is comprised of and no experimental tool existed to search exactly for the layer of a tiniest flake that is just an atom thick. It was finally spotted, thanks to the optical effect it creates over the top of SiO_2 substrate that makes it viewable through the simplest optical microscope. Hence we can deduce that it is rather difficult to find than to fabricate it. Firstly, we shall discuss about the fabrication methods and then move on to the characterization methods used to analyse the fabricated graphene samples.

3.2 Novel Approaches

3.2.1 Top-down approach: The fabrication of graphene involves two basic approaches – Top-down approach (large scale exfoliation) and the bottom-up approach (large scale synthesis). The top-down approach is the one in which the individual layers are peeled off or separated from the host molecule. This approach has been studied extensively by the researchers previously – Preparation of graphene from the Graphene Intercalation compounds, Graphene oxide or Graphite Oxide (discussed earlier) which includes chemical exfoliation – which follows a sequential process of oxidation of graphite, exfoliation of graphite oxide and reduction of the graphene oxide, thus obtained[18, 44-48], liquid phase exfoliation – exfoliation of graphitic materials in chemical solvents[49, 50], preparation of precise graphene nanoribbons by unzipping the carbon nanotubes (Fig 5) [51-55], that are considered as the rolled sheet of graphene longitudinally and the popular micro-mechanical exfoliation of graphite compounds like Highly Ordered Pyrolytic Graphene using a scotch-tape resulting in graphene formation[15].

Mechanical exfoliation when compared with liquid phase exfoliation provides single or few layer graphene with much higher quality, although the quantity will be considerably lower. The concept of mechanical exfoliation was further refined and highly ordered patterns of graphene were developed by Stamping and nanoimprinting, which offers better control and scalability than the conventional exfoliation process. In this method, a stamp is pressed onto the graphite substrates to cleave the

graphene islands and then the stamp with the cleavages of graphene is imprinted onto the device-ready substrates. The stamps used to imprint on the graphite substances are Si/SiO_2 pillars prepared by patterned plasma etching[56] (or) gold film stamp[57] (or) PDMS[58] (or) graphite[58]. A typical mechanical exfoliation, stamping and nanoimprinting process is illustrated in Fig 6.

Also, some more variations have been proposed for these exfoliation methods like the extraction of single layered graphene crystallites by rubbing a layered crystal against another surface (like drawing on a blackboard using chalk)[42], Electric field assisted Exfoliation[59, 60], exfoliation of oxidised graphite with the use of strong acids by rapid thermal expansion[61] or by ultrasonic dispersion[62]. Although this top-down approach is very simple, it has a major disadvantage that it does not offer any control over the process. Hence it is not possible to get the graphene of the desired quality or with a particular number of layers.

3.2.2 Bottom-up approach: The bottom-up approach, on the contrary, is based on the deposition of the material from the scratch and it is done in a controlled environment – with controlled parameters like temperature, pressure, flow rate and so on. Hence it is possible to get a defect-free graphene with the desired number of layers that can be employed in utilizable applications. The techniques that use this approach are epitaxial growth[41], High temperature annealing of single crystal SiC[63-65], Molecular Beam Deposition[66] under Ultra High Vacuum – evaporation of atomic carbon and subsequent annealing, Solvothermal synthesis[67] – High temperature thermo-chemical decomposition of a solvothermal or hydrothermal product, Chemical Vapour Deposition (CVD)[29, 68-72] and so on.

The epitaxial growth and the CVD are more or less the same, except for the type of growth of materials over the substrate. That is, for the epitaxy, the material is deposited such that the material takes up the same crystalline form as that of the substrate onto which it is deposited. In other words, the layer formed from the epitaxy is just another extension of the crystalline substrate. But for the CVD, the material can be deposited even on single layer crystals and can be independent of the substrate. Hence the Chemical Vapour Deposition has its edge over the other synthesis methods. The synthesis of high quality graphene has remained a consistent quest for over 30 years. Many refined CVD methods[73-76]

have recently been proposed after numerous researches being done on the fabrication of thin layer graphite films. However the graphene formed from Chemical Vapor Deposition requires post processing - transferring the films to other substrates[73, 74, 77] to make it device-compatible.

CVD is the decomposition of chemical precursors (in vapour state) over a heated substrate to yield a non-volatile solid thin film. Based on the reaction conditions and the chemical precursors used, the films may be epitaxial, polycrystalline or amorphous films. CVD enables us to have deliverables with high throughput, better purity, highly directional and also three dimensional structures with large aspect ratios, which make it attractive for large scale synthesis of thin films. However the quality of the films depends on the deposition variables like temperature, pressure, flow rate, precursor gases concentration, duration of heating, cooling rate, and so on.

The graphene formation by CVD basically involves two major steps: Pyrolysis of precursor chemicals to form carbon and settling of the dissociated carbon atoms to form a graphenic structure. But prevent the slightest possibility of clustering of carbon atoms (soot-like formation) onto the fabricated graphene, the pyrolysis should be done only on the substrate surface (heterogeneous decomposition). For heterogeneous decomposition to take place, transition metals are used as catalysts. The addition of catalysts also lowers the temperature range (from 2500^{o} C to around 1000^{o}C) and the energy consumption for achieving a good quality graphene, by reducing the energy barrier of the reaction. Based on the catalyst used, the graphenization mechanism differs as surface deposition (for Cu[78-81]) and surface segregation (for Ni[73, 74, 77, 82]) shown in Fig 7.

The kinetics of the CVD can further be detailed as,

- Pressurised gas lines supply the input reactant gases to the reaction chamber
- Mass transport of reactant gases from flow area to the substrate through the boundary layer (1)
- Adsorption of the precursor atoms on the surface of substrate, due to heating (2)
- Chemical reaction on the surface (3)
- Diffusion of atoms on the substrate to the nucleation sites (grain boundaries)
- Removal of the left-over gases and sludge resulting from the reactions (4)

- Mass transport of the exhaust gases to the flow area (5)

A typical illustration of kinetics of the CVD process is presented in Fig 8.

Types of CVD processes used

The three commonly used CVD processes for fabricating graphene are: Ambient Pressure CVD (APCVD)[73, 74, 82-85], Low Pressure CVD (LPCVD)[78, 86], and Plasma-Enhanced CVD (PECVD)[87-91]. The working principle is same for all the processes, but each process differs by a small streak of line by their working conditions. The comparisons of these three CVD process are presented in Table 2. APCVD systems, as their name suggest, are operated under normal atmospheric pressure conditions. They allow for high throughput and even continuous operation, while LPCVD operates at low pressures and it yields superior conformal step coverage and better film homogeneity. PECVD lowers the temperature to about 250 ^{o}C and hence it is used when lower temperatures are required. The deposition time is shorter (< 5 mins) but the film quality is often poor.

Variables affecting Deposition:

The three factors that affect the growth rate of the film are the feed rate of the inlet gases, the degree of diffusion and the surface kinetics. Then again the deposition rate of the film and the quality depends on the deposition variables (temperature, pressure, flow rate, cooling rate, concentration of the gases involved, etc.) In general, the deposition rate varies directly with temperature and follows the Arrhenius equation, $R = A \exp(-E_a/kT)$, where R is the deposition rate, E_a is the activation energy, T is the temperature (K), A is the frequency factor, and k is Boltzmann's constant (1.381 x 10-23 J/K).

Table 3 exhibited the comparisons of various graphene fabrication methods. At the high temperatures the rate of deposition is limited by the mass transport which implies that the rate of surface reaction is faster than the rate at which inlet gases are moved to the surface. In certain cases, the ratio of partial pressure of each of the reactants also plays a crucial role. The concentration level of the carbon supplying precursor for example, methane and the cooling rate also affect the deposition rate. For instance, if too low a concentration or too high a cooling rate will hinder the graphene growth. Now

with the deposition of graphene over the substrate, we need to confirm whether what we have, is graphene or not. For that we have a lot of characterization techniques to probe with.

4. CHARACTERIZATION TECHNIQUES

Graphene is one of the thinnest materials of the world with its dimension ranging from the size of nanometers to tens of microns, the prevalent mode of characterization is the microscope imaging techniques. The aim is to find the number of layers, single layers in specific, and to position and locate the layers over the given substrate, and to find their respective sizes.

The characterization can be majorly categorised based on the application they are used for – Structural and elemental analysis (Imaging or Analysis). The structural analysis as their name suggests is used to image the structure, "spot" it, and deduce important information pertaining to the functionality and that affects the property of the surface – such as number of layers, defects, chemical impurities, crystallite size, and so on. The elemental analysis of graphene gives us a storehouse of information on qualitative (the elemental structure) and quantitative (how much of each element) are present. The techniques engaged in the structural and elemental analysis are optical microscopy, scanning probe microscopy, Raman spectroscopy, Low Energy Electron Diffraction[26, 27, 37, 92-100] (LEED), Low Energy Electron Microscopy[65, 101] (LEEM), Reflective High Energy Electron Diffraction[102] (RHEED), etc. The summary of graphene characteriazations technologies including mechanism, speed, subtracts requirements and the types of analysis are presented in Table 6.

4.1 Optical Microscopy

A simple, sensitive, non-destructive and a fast technique among the very many ones existing for materials imaging is probably the optical microscopy. Finding a single layer of graphene in the sample is equivalent to finding a needle in a haystack, which makes the optical microscope observation tedious. The refractory index or the optical density of the mechanically exfoliated graphene is found to be 2.3% per single layer in the visible range[103, 104]. Under the bright field transmitted illumination, the optical images of graphene layers can generally be seen.

Also, it has been found that the incorporation of dielectric substrate between the material and a reflective surface enhances the visibility of monolayers through the optical microscope using fluorescence interference-contrast (colour change)[105]. This visibility phenomenon is basically because of the contrast that occurs from the interference of the reflected optical radiations at the interfaces of air-graphene, graphene-dielectric (e.g. Graphene – SiO_2), dielectric-substrate (e.g. SiO_2 – Si)[106]. SiO2 and Si3N4 are the widely used dielectric substrates over silicon wafers for enhancing the contrast of graphene layers[107]. Plus it has been reported that a triple layer system gave better contrast compared to a double layered system. In other words, the insertion of a thin dielectric between the graphene and a substrate yielded better results over a single bulk dielectric substrate[108]. However, on the deposition of graphene over substrates, there is a possibility of the absorption of optical radiation by the free atoms in gaseous state over a considerable wavelength range, the effect being called broadband absorption by molecular species. This makes it difficult to identify the graphene layers over the substrate. The major factors affecting the contrast have been analysed to enhance the clarity of the optical imaging and are found to be type of light source, intensity of light source, wavelength of the light source, thickness of specimen (graphene), dielectric material, thickness of dielectric film, substrate used with dielectric film, angle of incidence at the air-graphene interface, angle of incidence at the graphene-dielectric interface and optical absorbance of specimen and substrate[107-109]. It was also proved that the visibility of graphene depends on the thickness of the dielectric substrate used and the wavelength of light. For a particular thickness, even a monolayer offers a feeble yet sufficient contrast to locate the graphene crystallites from the graphitic sheets. Even a 5% deviation in thickness of the SiO_2 can make the graphene invisible[12].

Various optical methods employing reflective lighting techniques based on interferometry[15, 42, 106, 109-112], ellipsometry[113, 114], Rayleigh scattering[115], Fluorescence Quenching Microscopy[116, 117], Broadband spectrophotometry[118] and so on were proposed for better contrast optical imaging of graphene.

Interference techniques have been in use for over a century for the characterization of materials. By applying few modifications in the parameters involving interferometry techniques, the contrast level and

the resolution of the microscopy have been improved. This technique facilitates the visibility of graphene crystallites by utilising the phase contrast that occurs due to the small phase shifts in the light passing through the transparent graphene flakes that yields some colour changes in the optical image with respect to an empty wafer and substrate of appropriate thickness[15].

Ellipsometry, on the other hand, is yet another effective and non-destructive testing for the determination of optical constants and thicknesses of the thin films. In particular, imaging ellipsometry has proven its usefulness for the determination of such parameters[114, 119]. Unlike interferometry, this method measures the change in polarization state of the reflected light from the surface of the sample and it is very accurate, highly sensitive and reproducible even in low light levels. An elucidation showing the characterization using the spectroscopic ellipsometry (a & b) and imaging ellipsometry (c & d) has been made in Fig 9.

Rayleigh imaging involves the basic elastic Rayleigh scattering of photons. The elastically scattered photons provide another very efficient and quick way (since they form the majority of the reflected photons), to identify single and multilayer specimens and a direct way to measure their dielectric constants[115] and also for the probing of size, shape, concentration and optical properties of nanoparticles[120, 121]. Fluorescent Quenching Microscopy[116] is a relatively new technique for the imaging of graphene and graphene based sheets. Unlike the other optical methods which illuminate graphene and make them bright, this one utilizes the strong quenching effect of the fluorescent dyes, which when coated on graphene, upon excitation could reveal the underlying graphene as dark sheets in a bright background as illustrated in Fig 10. The advantages and disadvantages of optical microscopy are discussed in Table 4.

4.2 Scanning Probe Microscopy

Scanning probe microscopy (SPM) has facilitated the researchers for imaging material surfaces at nano-scale resolutions with relative ease. The accurate height measurements in nano-scale have in turn provided a direct probe of the number layers in graphene. The advantages and disadvantages of optical microscopy are summarized in Table 5.

(i) Scanning Tunnelling Microscopy (STM):

Scanning Tunnelling Microscopy is used when atomic scale resolution is needed[122]. Images of graphitic materials with atomic resolution that are taken using STM[123] are shown in Fig 11. The STM is based on various principles like: (1).Tunnelling of electrons – It is of general view that an object impinging an impenetrable barrier will not pass through. On the contrary, objects with relatively negligible mass, such as the electrons, having wave-like characteristics permit such an event, referred to as tunnelling. The tunnelling current depends exponentially on the tip-surface distance, making it a sensitive measuring device. This effect helps us to "see" the surface. (2) Piezo-electric effect – This effect assists in a precise control of scanning of material surface with the tip at sub-nanoscale levels. (3) Feedback control – This loop allows to monitor the tunnelling current and to manipulate the positioning of the probe-tip accordingly.

(ii) Atomic Force Microscopy (AFM):

Atomic Force Microscopy is used to measure the interaction force between the tip and sample surface which is eventually detected by a deflection of the cantilever holding the probe tip, or by a change in the resonant frequency of the cantilever. This technique overcomes the major drawback of STM the capability of which is restricted to imaging only the conducting and semi-conducting surfaces.

The common materials used for micro-fabrication of probe tips and cantilevers are Si or Si_3N_4. The force can be found using Hooke's law: $F = -kx$. It has been found that the attractive mode of AFM has a significant influence on the determination of the thickness of the graphene layers[124]. Besides imaging and thickness detection, AFM is very useful for characterizing the physical properties of graphene such as mechanical[125], frictional and elastic properties[126], electric and also magnetic properties, as it can resolve the small forces involved in the deformation process.

Some variants of the AFM process have also been employed in the characterization of graphene are: Force Modulation Microscopy – Elastic properties, Kelvin Probe Microscopy – Surface potential, Electrostatic force Microscopy – Charge Distribution, Lateral force Microscopy – Frictional Properties, Scanning Thermal Microscopy – Heat Conductivity within the graphene film and heat transfer to the

substrates lying beneath it and Ultrasonic Force Microscopy – Here the cantilever beam is made infinitely rigid utilising the very high frequency ultrasonic vibrations which in turn is used to find the elastic moduli of materials ranging from soft to hard. The vibrations are detected due to the non-linearity of the nanoscale contact of the tip and the sample. Also, this mode has a unique feature called ultrasonic superlubricity (zero friction between the tip and the sample), that prevents the damage to the tip and the sample.

4.3 Raman Spectroscopy

Raman spectroscopy is a form of vibrational spectroscopy similar to infrared (IR) spectroscopy. The difference lies in the fact that the Raman bands arise from the change in the polarizability whereas the IR bands originate from a change in the dipole moment of molecule. It is a powerful tool widely used for the imaging of graphene and graphene based materials. It provides better insight into the behaviour of phonons and electrons inside the sample, which in turn provides with versatile information about various parameters like crystallite size[127], clustering of the sp2 phase (which helps to deduce optical and electronic properties[128]), doping[129, 130], crystal defects[131], disorders[129, 132, 133], chemical impurities[134], edge chirality and crystal orientation[135], strain[136], thermal conductivity[137] and most importantly the number of graphene layers, stacking order and quality of the number of layers[138-140].

The Raman fingerprints prove to be a very resourceful tool if we know where exactly to look at. While discussing about the bands in the spectrum, three bands are extensively used, namely G-band (at ~ 1583 cm^{-1}), D-band (at ~ 1350 cm^{-1}) and 2D-band (at ~ 2680 cm^{-1}). There are other very small bands like D'-band (at ~ 1620 cm^{-1}) and D+G band (at ~ 2947 cm^{-1}). However they offer less significant details when compared the previous ones. Let us have a closer look at each of the bands. The Raman spectra for different number of layers for graphene is shown in the Fig 12.[141] The Raman spectra for various materials like graphite, single layer graphene (SLG), metallic and semiconducting carbon nanotubes, low and high sp^3 amorphous carbons, and diamond have been demostrated.

The G-band

The G-band is the primary mode in the graphene and graphite which is due to the E2g state phonon in the Γ-point in the Brillouin zone. This highly intense band arises from the stretching of C-C bond and it represents the planar configuration sp^2 bonded carbon that forms the foundation of graphitic systems. The position of the band is quite independent of the excitation laser frequency unlike the other Raman modes of graphene.

A great deal of information can be extracted out of this band if we know the band position and its shape. The band position is highly sensitive to strains and doping, which can be used to probe the surface features of the graphene – whether it is flat or not. Another common application is finding the graphene layer thickness with respect to the band position. The band position shifts to the lower energies as the layer thickness increases – a representation of the softening of bonds as layer thickness increases.

The D-Band

The D-band is commonly known as the disorder band since it is caused by the disordered structure of graphene. This band occurs due to the interactions of the localised vibration modes to the extended phonon modes of graphene. This band generally does not occur explicitly in graphene or graphite. For this band to be activated, it needs to be a defect or a graphene edge. If its presence is significant, then that is a direct implication of the presence of defects in the specimen. To the contrary, if the structure is perfect, there will be no D-peak. For this reason, this band is also referred to as the defect band.

The intensity of the D-band directly varies with the level of defects in the material. This band exhibits a dispersive behaviour – possesses weak sub bands within itself. Various underlying modes can be enhanced by using excitation lasers. Here both the band position and the shape depend on the laser excitation frequency. Hence it is to be ensured that the same excitation frequency is used for all the measurements while characterizing the D-band.

The 2D-Band

Commonly referred to as the overtone of the D-band or the G' Band, this band is the second order incarnation of the D-Band. All sp^2 hybridised carbon materials exhibit the very high intensity or a strong

peak in the interval of this spectrum (2500 cm^{-1} – 2800 cm^{-1}). It is a two phonon vibrational process and this mode does not need defects at its proximity to be activated, making it gaining an edge over the D-Band. This is used to determine the layer thickness like the G-Band but however this is not as simple as a band shift in the G-Band. With the increase in layer thickness, not only is there a shifting, but also there is a considerable change in the shape of the band which is attributed to the active components involved in the vibration.

For a single-layer Graphene, there is only a single component in the spectrum; whereas for a bilayer graphene, four components are present in the 2D-band.[142] It has a strong frequency dependence on the excitation laser energy and so the band position and the shape can vary significantly with various excitation lasers used. It is important that the same excitation frequency is used throughout the process. It is to be noted that the 2D-Band is sensitive to graphene folding. This band along with the G-Band forms the Raman signature of sp^2 materials. Raman spectrum of 2D band of graphene on Si/SiO_2 substrates as a number of layers changes from one to five is illustrated in Fig 13.

4.4 Others

The following passage explains some of the techniques used for the structural and elemental analysis of graphene and what information is extracted using those techniques.

1. X-Ray Photoelectron Spectroscopy (XPS)[65] – Measure elemental composition, empirical formula, chemical and electronic states of the particles in a material.
2. Auger Electron Microscopy (AES)[28-30, 143] – Quantitative determination of elements and its atomic concentration on material surface, qualitative fingerprinting spectral analysis, depth profiling and interface analysis.
3. Ultraviolet Photoelectron Spectroscopy (UPS)[69] – Determination of molecular energy levels in the valence band using the kinetic energy spectra of emitted photoelectrons.
4. Ion Scattering Spectroscopy (ISS)[144] – Determination of structure and composition of a substance, addressing catalytic surfaces, thin film coatings, adhesion, as well as arrangement of surface atoms.

5. Electron Energy Loss Spectroscopy (EELS)[76] – Measurement of atomic composition, chemical bonding, valence and conduction band electronic properties, surface properties, and element-specific pair distance distribution functions.
6. High Resolution Electron Energy Loss Spectroscopy (HREELS)[145-153] – Investigation of surface structure, catalysis, dispersion of surface phonons and the monitoring of epitaxial growth
7. Electron microscopy –For probing the surface features of materials using surface imaging technique.
8. Energy Dispersive X-Ray Analysis (EDX) in SEM[154] – Particle sizing, examination of surface morphology and characterization i.e. structural analysis, defect and failure analysis.
9. Nuclear Magnetic Resonance (NMR) Spectroscopy[49] – Determination of structures
10. Angle Resolved Photo Emission Spectroscopy – to analyse the electronic structure of graphene and using this method, the massless Dirac fermions are confirmed to exist[101, 155, 156].
11. Low Energy Electron Microscopy[65, 101] (LEEM) – Investigation of surface crystallography.
12. Low Energy Electron Diffraction[26, 27, 37, 92-100] (LEED) – For investigating the crystallography of surfaces and overlayers or films adsorbed on surfaces.
13. Reflective High Energy Electron Diffraction[102] (RHEED) – For probing the surface structures of solids.

5. APPLICATION POSSIBILITIES

5.1 Electronic device

Graphene is considered to be capable of outdating the Si based electronics and form the post Si era of electronics due its superior transport properties. Various graphene nano-electronic devices have been fabricated[10, 157-159] and there has been a constant probing towards the application oriented fabrication ever since.

5.1.1 Transistors

Transistors made out of graphene have been reported to have hole and electron mobility of about 3735 cm^2/Vs and 795 cm^2/Vs with the highest ever reported maximum drive current at room temperature[56]

(1.7 mA/μm at V_{ds} = 1V) and an intrinsic cutoff frequency of up to 300 GHz has been demonstrated[160]. Its potential incorporation into the radio-frequency based applications has called for a great interest in the fabrication of transistors using graphene[161-165].

5.1.2 Plasmonic device – terahertz plasmon oscillators[166, 167]

The simulation of energy band of graphene with absorption and emission of plasmons are illustrated in Fig 14. By inversely populating the graphene layers and by coupling the plasmons (a quantum of plasma oscillations – self-sustained collective oscillations of conduction electrons) with the interband electron-hole transitions in those layers, it is possible to facilitate the plasmons to experience very large gains through a stimulated emission process. The plasmon amplification with even a small excitation is considered to occur when the frequency of the exciting light field is in resonance with the Eigen frequency of the collective oscillation of electrons.

The concept of obtaining negative conductivity in graphene at terahertz frequencies, which necessitates for the population inversion through optical and electrical pumping, has been discussed extensively. The same concept has been extended to design plasmon oscillators wherein the graphene strips act as the plasmon cavity and the pumping assist with the electron-hole recombination. A schematic illustration of a graphene terahertz oscillator under load is given in the Fig 15 (a). Also under negative impedance conditions while under population inversion, the graphene strip can be used for terahertz amplifiers shown in Fig 15 (b).

5.1.3 Ultrafast lasers

Graphene due to its non-linear and electro optical properties is used in the field of nano-photonics, in particular, the ultra-fast lasers (nano to sub-picosecond pulses). In a laser optical cavity (an arrangement of mirrors) the mirror-like arrangement takes care of the light emission at well-defined wavelengths, known as modes. Each mode oscillates with a different phase in due course of time. When these modes superimpose with each other, they form constructive and continuous laser waves.

Non-linear optical elements called saturable absorbers are selective laser absorbers that absorb only the laser with higher intensities, damp the lower intensity laser waves. When all these modes with strong

intensity oscillate in phase after undergoing many repeated circulations inside the cavity, the continuous wave output is converted into a train of short and intense (pulsed) waves. A wideband tuneability can be obtained when graphene is used as the saturable absorber due to its zero band gap and significant optical absorbance[168]. Whereas the conventional, semiconductor saturable absorbing mirrors require band gap engineering for utilising them in ultra-fast lasers.

An example of the mode locking laser using graphene has been illustrated in the Fig 16. Here, the graphene/PVA (Poly-Vinyl Alcohol – host polymer) based saturable absorber is slid and sandwiched between two fibre connectors. The gain medium used for this laser is Erbium Doped Fibre (EDF) and the pumping is made possible through a Diode Laser (Pump Laser) by means of a Wavelength Division Multiplier (WDM). To maintain a unidirectional operation, an Isolator (ISO) is used and to have an optimized mode-locking, a Polarization Controller (PC) is used. Graphene ultra-fast photonic devices[169] have been demonstrated out of graphene[170-174], Graphene-Polymer nanocomposites[169, 171, 174-177], Solution processed graphene[178-180] and so on.

5.1.4 Spintronic device[181, 182] – digital memory devices[183]

The electronic devices that utilize the quantum spin of the electrons, instead of the conventional way of using electric charges to process information, are termed as spintronic devices. The recent experimental observations report magnetism in graphitic materials which was considered unlikely in the carbon based systems due to their lacking of *d* or *f* electrons. This has led to a surge in the research of graphene based novel spintronic devices wherein the graphene helps integrating the nanoscale quantum properties with device environments, due to their particular combination of high 2D aspect ratios with unique conductivity properties, such as bipolar tunability of charge and high mobility along with the expected long spin coherence lifetimes and lengths[181].

Also, the vacancies in graphene have found to be acting as tiny magnets themselves since they have magnetic moment[184]. Various assumptions that are expected to bring out spin current in graphene and making it magnetically active. One idea is through spin splitting in monolayer graphene using the magnetic properties of graphene (ferromagnetic proximity effect) and adiabatic quantum pumping[182].

The second idea is by shaping the graphene (say, a single walled carbon nanotube of few nanometers in diameter), the spin is strongly affected by their motion as they are forced to move around the tube[185]. Other ideas include using Graphene-Magnet Multilayers (graphene brought in contact with magnetic and non-magnetic layers)[186] and by properly arranging the magnetization of the magnetic layers, by localizing spin polarization at one dimensional zigzag edges of graphene[187-190].

A hybrid spintronic nano-device has been developed by functionalizing magnetic particles over a planar sheet of graphene[181] to trap the molecules chemically, capture the magnetic flux, and to generate a corresponding electric signal, thereby measuring even the tiniest of magnetic signal down to molecular levels (Fig 17).

5.1.5 Quantum computing[191],

When the term quantum computing is used, a spin quantum bit (qubit) will be considered equivalently. The relative spin of electron localized in semiconductor quantum dots with proper position and orientation control, can be utilized as carriers of quantum information in the quantum computers. These qubits require materials with weaker spin-orbit coupling and hyperfine interactions of the electron spins with the neighbor nuclear spins. Carbon based materials have weaker spin-orbit coupling and hyperfine interactions because of their lower atomic weights and atomic constituents. Also the spin polarization in the graphitic materials decays more slowly resulting in long term information storage.

But because of the absence of band gap in the electronic spectrum and the klein tunnelling it is very difficult to confine particles and form tunable quantum bits using graphene and due to the valley degeneracy, it is difficult to form two qubit gates using Heisenberg exchange coupling. By overcoming the above said limitations, a method has been proposed to form the spin qubits in graphene quantum dots with armchair boundaries. The system is developed based on graphene nanoribbons with semiconducting armchair edges[192] as shown in Fig 18.

The confinement is achieved by tuning the applied voltage to the barrier gates (indicated in blue). To shift the energy levels of the dots, additional gates (indicated in red) have been introduced. Universal two-qubit gates have been generated by the tunable exchange coupling formed between the left and the

right quantum dots due to the virtual hopping of electrons through the barrier 2. This system so formed can be used for fault tolerant computations offering low error rates and high error thresholds.

5.2 Optoelectronic Device

Graphene based transparent conductive films have been employed in Optoelectronic devices[111, 193]. Although the graphene has superior optical properties, the major hurdles faced by the implementation of graphene in optoelectronics are the higher sheet resistance offered by the graphene prepared by CVD techniques (approximately 280 $\Omega\,\square^{-1}$) compared to the ITO (100 $\Omega\,\square^{-1}$), the robust substrate requirements to withstand higher temperatures and the transfer of the graphene films onto the foreign substrates.

5.2.1 Touch screen

Two major types of the touch screens have been employed in the industries – resistive and capacitive touchscreens [169, 194]. The resistive touch screens are majorly classified as matrix and analogue type. The former has the a matrix like structure where the patterned electrodes over substrates like glass or plastic face each other, whereas for the latter, the transparent electrodes just face each other without the need of patterning. And the analogue type touch screen continuous change in resistance and the resistance needs to be high as well (500–2000 $\Omega\,\square^{-1}$). The schematics for both these types have been given in the Fig 19.

The capacitive touch screens, on the other hand, utilizes the electrostatic field distortion induced by the touching of screen and converts it into a measurable change of capacitance. Graphene based Transparent Conductive Films offer higher sheet resistance and better transparency along with a long range uniformity when compared to the conventional films based on ITO. A schematic of capacitive touch screen is given in Fig 20.

The previously discussed limitations were overcome by a roll-to-roll production of high quality graphene [194] which involves three major steps – attaching polymer to the graphene together onto the copper foil, etching of the copper layers and releasing graphene layers and transferring onto a target substrate shown in Fig 21. In the attachment of polymer support and graphene onto the copper foils, the

graphene film deposited on a copper foil, is attached to a thin polymer film coated with an adhesive layer by passing between two rollers.

5.2.2 FE displays

Field Emission (FE), as its name suggests, is an electron-field emission process in which electrons are emitted from a material induced by a high electrostatic field. The simplest way to attain such a field is by making the electron emitter a sharp pointed tip of a sharp object (called as field emitter) and through its field enhancement. Graphene can be used as a field emitting structure as long as the FLG density is controlled, since it might cause a field screening effect. Graphene electrodes prepared out of spin coating the graphene oxide dissolved in polystyrene[195], electrophoretic deposition[196], thermal CVD[197] and Micro Wave Plasma Enhanced CVD (MW-PECVD)[198] have been reported to have provided good quality suitable for the FE based applications.

5.2.3 Light Emitting Diodes[84]

Graphene could be made luminescent by inducing a band gap through either physical or chemical treatments, or through the alteration of graphene into nanoribbons or quantum dots. When made electro-luminescent (combining the luminescence and the conductive layers together), graphene can be clubbed together to form Light Emitting Diodes. An Organic Light Emitting Diode (shown in Fig 22) has an organic light emitting layer sandwiched between two electrodes that inject holes and electrons to the orbitals of the anode (highest occupied molecular orbital) and cathode (lowest unoccupied molecular orbital) respectively.

The traditionally used material for the OLED's, is the ITO with a work function of about 4.4-4.5 eV. But it provides with only limited flexibility and the diffusivity of Indium into the OLED layers affects the performance of the devices. Since graphene also has the same range of work function of about 4.5 eV and it has better flexibility, it can be considered as an excellent alternative for the ITO based OLED's.

5.2.4 Light-bending switchable graphene metamaterials

Metamaterials are a new generation materials with dimensions much smaller than the relevant wavelength and display distinct optical properties, mostly associated with negative refraction. This property can be utilized in sensing devices, high resolution microscopy, invisibility cloaks, and so on. Metamaterials are to the artificially arranged structural elements, as the matter is to the atoms that constitute it. By using the properties like renormalisation of plasmonic modes and frequency shift of the trapped-mode transmission resonance in the presence of the highly polarizable graphene, a photonic device has been developed based on graphene over metamaterials[199].

The device is built using a two-dimensional array of asymmetrically-split ring slits on a gold film. Metamaterials have the so-called characteristic Fano anti-symmetric resonant lines in transmission with enhanced local fields which is responsible for the high contrast detection of graphene as well as the sensing applications based on metamaterials. In this setup, the graphene acts as a continuous adsorption layer. Addition of the graphene to metamaterial results in a dramatic change of the transmission spectrum and a 250% increase in the transmission is observed.

5.2.5 Transparent conductive device

Transparent conductive devices made using large scale graphene[200, 201] can be used for flexible (stretchable) electronics. The optical absorbance of only 2.3% of the total light makes graphene one of the most transparent conductors reported so far. Indium Tin Oxide (ITO), the conventional material for the transparent conductors has now a superior alternative offering high performance[202], the graphene which can be used for the applications in transparent conductive devices.

5.3 Energy generation device

The long standing energy crisis has led to the constant probing into the alternate renewable energy source or that enhances the existing power generation capabilities. Graphene is a promising material for power generation and has been employed in the fuel cells[203-208], photovoltaic cells[209-213], possibly solar thermal fuel cells[209-213] as their tunable band gap and large optical absorbance are desirable for efficient light harvesting and their large carrier concentrations helps in the charge collection in the solar cells.

Photovoltaic cells are those devices which convert the light into electrical energy. The widely known photovoltaic devices are based on mostly the organic photovoltaic cells and dye-sensitized photovoltaic cells. The organic photovoltaic cells offer flexibility, good light absorption and charge transport but is limited by the polymer used compared to the inorganic cells (Fig 23 (a)). An organic solar cell consists of a transparent conductor, a photoactive layer and the electrode (Fig 23 (b)). The recent advancements in photovoltaic devices report a sub-category of the organic polymer based photovoltaic cells – quantum dot sensitized solar cells used as electron acceptor materials in photovoltaics.

Quantum dots have beneficial properties – such as their size-tuned optical response, efficient multiple carrier generation, and low cost – that make them attractive for photovoltaic devices. But the quantum dots that have been made so far, have toxic materials like Cadmium and Lead that would pose threat to the environment when we go far large-scale device applications. However, the devices made out of graphene quantum dots (GQD) are not toxic but still offer similar electronic properties suitable for the photovoltaic device applications. Also its high charge carrier mobility results in a quick transport of charges to the electrodes, which in turn means reduction in current losses and improvement of solar cell efficiency. Also it has been found that, when combined with a conjugated polymer, the graphene quantum dots exhibit superior functionality when compared with graphene sheets that are blended with the same polymer.

The other major category is the dye-sensitized solar cells (Fig 23 (c)) which use a liquid electrolyte as charge transport medium. These cells consist of highly porous nano-size crystalline photo-anode, comprising TiO_2 and dye molecules, both deposited on a transparent conductor. When light is incident on these cells, the dye molecules capture the incident photons and generate electron–hole pairs. The electrons are injected into the conduction band of the TiO_2 and then moved to the other electrode. Regeneration of dye molecules occur by capturing electrons from the liquid electrolyte. ITO is the commonly used material finding its applications as an anode and a cathode; for its use as cathode requires platinum coating. In photovoltaic devices, graphene is multifunctional and finds its functions as the transparent conductor window, photoactive material, channel for charge transport, and catalyst.

5.4 Energy storage device

With the ever increasing demand for the electronic and energy generation devices, there exists an equal constant demand for the energy storage. Ultracapacitors or electrochemical capacitors based on electrochemical double layer capacitance (EDLC) are good electrical energy storage devices that stores and releases energy by nanoscopic charge separation at the electrochemical interface between an electrode and an electrolyte[214]. These ultracapacitors offer high energy density, high power capability, long life and low weight compared to the conventional dielectric capacitors. They consistently give a good performance and reliability over a wide range of voltage scan rates for short load cycles with graphene as the electrode materials[215-217].

The nearly negligible effect of thermal vibrations on the electron conduction in graphene and hence the very low resistivity of about 1μΩ at room temperature (nearly 35% lesser than the resistivity of copper) makes this an interesting specimen for superconducting applications, although some extrinsic sources in the graphene with quite some impurities available at the present results in an added resistivity to the graphene[14]. Thus graphene finds its applications in energy storage, especially supercapacitors due to its high specific area and its supreme electron transport properties, when its individual monolayers are stacked onto one another and keeping the layers of the chemically modified graphene (CMG) wet[218]. Since graphene is an atom-level thick and having very low surface energy, it can be used to reduce the adhesion and friction while coating over various surfaces. It is the thinnest solid lubricant found so far and it shows exceptional adhesion and frictional characteristics when fabricated by the chemical vapour deposition over Ni and Cu catalysts[219]. Nano-electromechanical systems fabricated from single layer and multilayer graphene sheets by mechanically exfoliating thin sheets from graphite over trenches in silicon oxide, form the thinnest resonator consisting of a single suspended layer of atoms and represents the ultimate limit of two-dimensional nano-electromechanical systems[10].

Architectural graphene structures have been proposed to enhance the existing energy storage capacities. Nano-architecture pillared graphene when doped with lithium cations can store up to 41 g H_2/L under ambient conditions for mobile applications[220]. Graphene has also found its application in

batteries[203, 221-224](as the electrode materials) and flexible energy storage devices[225]. The proposed structure with a hybrid of graphene and CNT's has been shown in the Fig 24 (a). and the simulated illustration of graphene undoped storing hydrogen (green) and that of graphene doped with the lithium (purple) storing Hydrogen (green) is shown in Fig 24 (b) and (c). 3D foam like grapheme macrostructure can be directly grown on Ni foam. After chemical etching the Ni foam, 3D grapheme foam can be obtained with unique network structure and the outstanding electrical and mechanical properties (Fig 25)[226].

5.5 Bio-imaging and Bio-sensing applications

The chemical inertia and the non-toxicity in the physiological conditions call for the entry of graphene into the fields ranging from medical diagnosis to catalysis – in particular they are employed as effective fluorescent probes for bio-imaging[227-229].

The high sensitivity of graphene – up to the molecular level – a resolution that has been beyond the reach of any detection technique so far, has enabled its application in the field of electro-chemical[230-235] and bio-sensors[236, 237]. This high sensitivity and its ability to detect elements ranging from gases to biomolecules can be attributed to the variation of the electrical conductivity of graphene as the function of its surface adsorption[125] and its large specific surface area[12]. In general, the change in the conductance of the graphene is due to the change in charge carrier densities (carrier concentrations) induced by the immediate environment, in our case, acceptor or donor-like behaviour of the adsorbed gases depending on the interaction with the graphene lattice.

5.6 Environmental applications

Water dispersible graphene oxide nano-composite removes almost 99.9% of the toxic and carcinogenic Arsenic from the water within 1 ppb and hence can be employed in the water purification[238]. Ni-Doped graphene/carbon crygels exhibits 93% of the motor oil absorption capacity and maximum absorption capacity of 151 mg g^{-1} for organic pollutants (Methyl blue).[239] Reduced grapheme oxide-coated polyurethane sponge delivered oil absorption capabilities higher than 80 g g^{-1} and 160 g g^{-1} for chloroform. [240]

5.7 Biomedical applications

Paper-like materials formed using graphene have remarkable thermal, mechanical and electrical properties. Their biocompatibility and ease of handling make them an ideal material for cell culture experiments, biomedical applications like inclusion in heart valves[241], batteries[242, 243].

5.8 Other applications

An atomic level thick membrane of graphene is impermeable to almost all standard gases including Helium due to the electron density of its aromatic rings. This property allows us to measure the elastic constants and the mass of the graphene membranes. The single atomic layer membranes which when combined with the micro-fabricated structures can create a new class of atomic scale membrane based devices[11]. It has been demonstrated that robust atomic-level graphene membranes are capable of storing mesoscopic volumes of gases[244]. With this, it is possible to make pressure sensors, stretchable strain gauges[80], atomic-scale mechanical devices capable of gas storage and separation, proton exchange membranes for fuel cells, carbon sequestration from flue gases and so on[245]. Polymer based nano-composites offer enhanced gas barrier and mechanical properties[246] which when infused with graphene as filler material can revolutionize the food packaging and processing applications.

6. CONCLUSION

In summary, we have reviewed the principle and fundamental of exotic properties of graphene – the Dirac Fermions and the Dirac cone arrangement of its electronic structure, Quantum Hall Effect, Klein Paradox, Zitterbewegung effect, non-zero minimal conductivity, the fabrication approaches of graphene, characterization techniques for structural and elemental analysis, and finally the applications wherein the wonder material is employed in numerous applications (Fig 26). As illustrated in Fig 27 with the source of Web of Science & World Intellectual Property Office (WIPO), there is an exponential increase in the number of publications in this field and the interest is constantly growing. There has been a proportionate increase in the number of patents which proves that the industrial value of graphene is being exploited simultaneously. The quest for the perfection and more applications is still under further

investigation, which is why it is apt that the Graphene can be termed as the Philosopher's Stone of the Modern Ages.

Acknowledgement

Dr X. Zhang thanks the financial supported by Public Sector Research Funding (Grant number 1121202012), Agency for Science, Technology, and Research (A*STAR). Dr. H. Liu thanks the postdoc fellowship from Yong Loo Lin School of Medicine, NUS and Cardiovascular Research Institute, NUHS.

REFERENCES

1. R. S. HANNS-PETER BOEHM and E. STUMPP.
2. A. D. McNaught and A. Wilkinson, *Compendium of Chemical Terminology, 2nd ed. (the "Gold Book")*, 1997.
3. B.-C. Wang, H.-W. Wang, J.-C. Chang, H.-C. Tso and Y.-M. Chou, *Journal of Molecular Structure: THEOCHEM*, 2001, **540**, 171-176.
4. R. Peierls, *Helv. Phys. Acta*, 1934, **7**, 81–83.
5. R. Peierls, *Ann. Inst. Henri Poincare*, 1935, **5**, 177–222.
6. L. Landau, *Phys. Z. Sowjetunion*, 1937, **11**, 26–35.
7. N. D. Mermin, *Physical Review*, 1968, **176**, 250.
8. J. C. Meyer, A. Geim, M. Katsnelson, K. Novoselov, T. Booth and S. Roth, *Nature*, 2007, **446**, 60-63.
9. A. Fasolino, J. H. Los and M. I. Katsnelson, *Nat Mater*, 2007, **6**, 858-861.
10. J. S. Bunch, A. M. van der Zande, S. S. Verbridge, I. W. Frank, D. M. Tanenbaum, J. M. Parpia, H. G. Craighead and P. L. McEuen, *Science*, 2007, **315**, 490-493.
11. J. S. Bunch, S. S. Verbridge, J. S. Alden, A. M. Van Der Zande, J. M. Parpia, H. G. Craighead and P. L. McEuen, *Nano Letters*, 2008, **8**, 2458-2462.
12. A. K. Geim and K. S. Novoselov, *Nature materials*, 2007, **6**, 183-191.
13. E. Y. Andrei, G. Li and X. Du, *Reports on Progress in Physics*, 2012, **75**, 056501.
14. J. H. Chen, C. Jang, S. Xiao, M. Ishigami and M. S. Fuhrer, *Nature Nanotechnology*, 2008, **3**, 206-209.
15. K. S. Novoselov, A. K. Geim, S. V. Morozov, D. Jiang, Y. Zhang, S. V. Dubonos, I. V. Grigorieva and A. A. Firsov, *Science*, 2004, **306**, 666-669.
16. M. A. Rafiee, J. Rafiee, Z. Wang, H. Song, Z. Z. Yu and N. Koratkar, *ACS Nano*, 2009, **3**, 3884-3890.
17. M. A. Rafiee, J. Rafiee, I. Srivastava, Z. Wang, H. Song, Z. Z. Yu and N. Koratkar, *small*, 2010, **6**.
18. S. Stankovich, D. A. Dikin, G. H. B. Dommett, K. M. Kohlhaas, E. J. Zimney, E. A. Stach, R. D. Piner, S. B. T. Nguyen and R. S. Ruoff, *Nature*, 2006, **442**, 282-286.
19. C. Schafhaeutl, *Journal für Praktische Chemie*, 1840, **21**, 129-157.
20. P. Debye and P. Scherrer, *Nachrichten von der Gesellschaft der Wissenschaften zu Göttingen, Mathematisch-Physikalische Klasse*, 1917, **2**, 180-188.
21. B. C. Brodie, *Philosophical Transactions of the Royal Society of London*, 1859, **149**, 249-259.
22. B. Brodie, *QJ Chem. Soc.*, 1860, **12**, 261-268.
23. L. Staudenmaier, *Berichte der deutschen chemischen Gesellschaft*, 1898, **31**, 1481-1487.
24. W. S. Hummers and R. E. Offeman, *Journal of the American Chemical Society*, 1958, **80**, 1339-1339.
25. H. Boehm, A. Clauss, G. Fischer and U. Hofmann, *Ann. Chem*, 1934, **510**, 1.
26. A. Morgan and G. Somorjai, *Surface Science*, 1968, **12**, 405-425.
27. J. May, *Surface Science*, 1969, **17**, 267-270.
28. J. Hamilton and J. Blakely, *Surface Science*, 1980, **91**, 199-217.
29. M. Eizenberg and J. Blakely, *The Journal of Chemical Physics*, 1979, **71**, 3467.
30. J. Shelton, H. Patil and J. Blakely, *Surface Science*, 1974, **43**, 493-520.
31. A. Van Bommel, J. Crombeen and A. Van Tooren, *Surface Science*, 1975, **48**, 463-472.
32. D. V. Badami, *Carbon*, 1965, **3**, 53-54, IN55-IN58, 55-57.
33. C. Oshima, E. Bannai, T. Tanaka and S. Kawai, *Japanese Journal of Applied Physics*, 1977, **16**, 965-969.
34. R. Rosei, M. De Crescenzi, F. Sette, C. Quaresima, A. Savoia and P. Perfetti, *Physical Review B*, 1983, **28**, 1161.

35. N. A. Kholin, E. V. Rut'kov and A. Y. Tontegode, *Surface Science*, 1984, **139**, 155-172.
36. N. Gall, S. Mikhailov, E. Rut'kov and A. Tontegode, *Sov. Phys. Solid State*, 1985, **27**, 1410-1414.
37. H. Zi-Pu, D. F. Ogletree, M. A. Van Hove and G. A. Somorjai, *Surface Science*, 1987, **180**, 433-459.
38. T. Aizawa, R. Souda, S. Otani, Y. Ishizawa and C. Oshima, *Physical Review B*, 1990, **42**, 11469.
39. A. Nagashima, K. Nuka, H. Itoh, T. Ichinokawa, C. Oshima and S. Otani, *Surface Science*, 1993, **291**, 93-98.
40. X. Lu, M. Yu, H. Huang and R. S. Ruoff, *Nanotechnology*, 1999, **10**, 269.
41. C. Berger, Z. Song, T. Li, X. Li, A. Y. Ogbazghi, R. Feng, Z. Dai, A. N. Marchenkov, E. H. Conrad, P. N. First and W. A. de Heer, *The Journal of Physical Chemistry B*, 2004, **108**, 19912-19916.
42. K. Novoselov, D. Jiang, F. Schedin, T. Booth, V. Khotkevich, S. Morozov and A. Geim, *Proceedings of the National Academy of Sciences of the United States of America*, 2005, **102**, 10451.
43. Y. Zhang, Y.-W. Tan, H. L. Stormer and P. Kim, *Nature*, 2005, **438**, 201-204.
44. D. A. Dikin, S. Stankovich, E. J. Zimney, R. D. Piner, G. Dommett, G. Evmenenko, S. B. T. Nguyen and R. S. Ruoff, *NATURE-LONDON-*, 2007, **448**, 457.
45. V. C. Tung, M. J. Allen, Y. Yang and R. B. Kaner, *Nature Nanotechnology*, 2008, **4**, 25-29.
46. C. Gómez-Navarro, R. T. Weitz, A. M. Bittner, M. Scolari, A. Mews, M. Burghard and K. Kern, *Nano Letters*, 2007, **7**, 3499-3503.
47. S. Park and R. S. Ruoff, *Nature Nanotechnology*, 2009, **4**, 217-224.
48. C. Vallés, C. Drummond, H. Saadaoui, C. A. Furtado, M. He, O. Roubeau, L. Ortolani, M. Monthioux and A. Pénicaud, *Journal of the American Chemical Society*, 2008, **130**, 15802-15804.
49. S. Stankovich, D. A. Dikin, R. D. Piner, K. A. Kohlhaas, A. Kleinhammes, Y. Jia, Y. Wu, S. T. Nguyen and R. S. Ruoff, *Carbon*, 2007, **45**, 1558-1565.
50. Y. Hernandez, V. Nicolosi, M. Lotya, F. M. Blighe, Z. Sun, S. De, I. T. McGovern, B. Holland, M. Byrne, Y. K. Gun'Ko, J. J. Boland, P. Niraj, G. Duesberg, S. Krishnamurthy, R. Goodhue, J. Hutchison, V. Scardaci, A. C. Ferrari and J. N. Coleman, *Nat Nano*, 2008, **3**, 563-568.
51. A. L. Elías, A. s. R. Botello-Méndez, D. Meneses-Rodríguez, V. Jehová González, D. Ramírez-González, L. Ci, E. Muñoz-Sandoval, P. M. Ajayan, H. Terrones and M. Terrones, *Nano Letters*, 2009, **10**, 366-372.
52. D. V. Kosynkin, A. L. Higginbotham, A. Sinitskii, J. R. Lomeda, A. Dimiev, B. K. Price and J. M. Tour, *Nature*, 2009, **458**, 872-876.
53. L. Jiao, L. Zhang, X. Wang, G. Diankov and H. Dai, *Nature*, 2009, **458**, 877-880.
54. A. G. Cano-Márquez, F. J. Rodríguez-Macías, J. Campos-Delgado, C. G. Espinosa-González, F. Tristán-López, D. Ramírez-González, D. A. Cullen, D. J. Smith, M. Terrones and Y. I. Vega-Cantú, *Nano Letters*, 2009, **9**, 1527-1533.
55. M. Terrones, A. R. Botello-Méndez, J. Campos-Delgado, F. López-Urías, Y. I. Vega-Cantú, F. J. Rodríguez-Macías, A. L. Elías, E. Muñoz-Sandoval, A. G. Cano-Márquez, J.-C. Charlier and H. Terrones, *Nano Today*, 2010, **5**, 351-372.
56. X. Liang, Z. Fu and S. Y. Chou, *Nano Letters*, 2007, **7**, 3840-3844.
57. L. Song, L. Ci, W. Gao and P. M. Ajayan, *ACS Nano*, 2009, **3**, 1353-1356.
58. M. J. Allen, V. C. Tung, L. Gomez, Z. Xu, L.-M. Chen, K. S. Nelson, C. Zhou, R. B. Kaner and Y. Yang, *Advanced Materials*, 2009, **21**, 2098-2102.
59. A. N. Sidorov, M. M. Yazdanpanah, R. Jalilian, P. Ouseph, R. W. Cohn and G. Sumanasekera, *Nanotechnology*, 2007, **18**, 135301.
60. X. Liang, A. S. P. Chang, Y. Zhang, B. D. Harteneck, H. Choo, D. L. Olynick and S. Cabrini, *Nano Letters*, 2008, **9**, 467-472.

61. S. Niyogi, E. Bekyarova, M. E. Itkis, J. L. McWilliams, M. A. Hamon and R. C. Haddon, *Journal of the American Chemical Society*, 2006, **128**, 7720-7721.
62. S. Stankovich, R. D. Piner, X. Chen, N. Wu, S. T. Nguyen and R. S. Ruoff, *Journal of Materials Chemistry*, 2006, **16**, 155-158.
63. C. Berger, Z. Song, X. Li, X. Wu, N. Brown, C. Naud, D. Mayou, T. Li, J. Hass and A. N. Marchenkov, *Science*, 2006, **312**, 1191.
64. W. A. De Heer, C. Berger and X. Wu, *Solid State Communications*, 2007, **143**, 92-100.
65. K. V. Emtsev, A. Bostwick, K. Horn, J. Jobst, G. L. Kellogg, L. Ley, J. L. McChesney, T. Ohta, S. A. Reshanov, J. Rohrl, E. Rotenberg, A. K. Schmid, D. Waldmann, H. B. Weber and T. Seyller, *Nat Mater*, 2009, **8**, 203-207.
66. J. M. Garcia, R. He, M. P. Jiang, J. Yan, A. Pinczuk, Y. M. Zuev, K. S. Kim, P. Kim, K. Baldwin and K. W. West, *Solid State Communications*, 2010, **150**, 809-811.
67. M. Choucair, P. Thordarson and J. A. Stride, *Nat Nano*, 2009, **4**, 30-33.
68. C. Oshima and A. Nagashima, *Journal of Physics: Condensed Matter*, 1997, **9**, 1.
69. R. Rosei, S. Modesti, F. Sette, C. Quaresima, A. Savoia and P. Perfetti, *Physical Review B*, 1984, **29**, 3416.
70. J. Wintterlin and M. L. Bocquet, *Surface Science*, 2009, **603**, 1841-1852.
71. A. N. Obraztsov, E. A. Obraztsova, A. V. Tyurnina and A. A. Zolotukhin, *Carbon*, 2007, **45**, 2017-2021.
72. P. R. Somani, S. P. Somani and M. Umeno, *Chemical Physics Letters*, 2006, **430**, 56-59.
73. K. S. Kim, Y. Zhao, H. Jang, S. Y. Lee, J. M. Kim, K. S. Kim, J.-H. Ahn, P. Kim, J.-Y. Choi and B. H. Hong, *Nature*, 2009, **457**, 706-710.
74. A. Reina, X. Jia, J. Ho, D. Nezich, H. Son, V. Bulovic, M. S. Dresselhaus and J. Kong, *Nano Letters*, 2008, **9**, 30-35.
75. H. Cao, Q. Yu, R. Colby, D. Pandey, C. Park, J. Lian, D. Zemlyanov, I. Childres, V. Drachev and E. A. Stach, *Journal of Applied Physics*, 2010, **107**, 044310-044310-044317.
76. A. Dato, V. Radmilovic, Z. Lee, J. Phillips and M. Frenklach, *Nano Letters*, 2008, **8**, 2012-2016.
77. Q. Yu, J. Lian, S. Siriponglert, H. Li, Y. P. Chen and S. S. Pei, *Applied Physics Letters*, 2008, **93**, 113103.
78. X. Li, W. Cai, J. An, S. Kim, J. Nah, D. Yang, R. Piner, A. Velamakanni, I. Jung and E. Tutuc, *Science*, 2009, **324**, 1312.
79. H. Cao, Q. Yu, L. A. Jauregui, J. Tian, W. Wu, Z. Liu, R. Jalilian, D. K. Benjamin, Z. Jiang and J. Bao, *Applied Physics Letters*, 2010, **96**, 122106.
80. Y. Lee, S. Bae, H. Jang, S. Jang, S.-E. Zhu, S. H. Sim, Y. I. Song, B. H. Hong and J.-H. Ahn, *Nano Letters*, 2010, **10**, 490-493.
81. X. Li, W. Cai, L. Colombo and R. S. Ruoff, *Nano Letters*, 2009, **9**, 4268-4272.
82. L. G. De Arco, Z. Yi, A. Kumar and Z. Chongwu, *Nanotechnology, IEEE Transactions on*, 2009, **8**, 135-138.
83. Q. Yu, J. Lian, S. Siriponglert, H. Li, Y. P. Chen and S.-S. Pei, *Graphene segregated on Ni surfaces and transferred to insulators*, AIP, 2008.
84. J. Wu, M. Agrawal, H. A. Becerril, Z. Bao, Z. Liu, Y. Chen and P. Peumans, *ACS Nano*, 2009, **4**, 43-48.
85. A. Reina, S. Thiele, X. Jia, S. Bhaviripudi, M. Dresselhaus, J. Schaefer and J. Kong, *Nano Research*, 2009, **2**, 509-516.
86. X. Li, C. W. Magnuson, A. Venugopal, R. M. Tromp, J. B. Hannon, E. M. Vogel, L. Colombo and R. S. Ruoff, *Journal of the American Chemical Society*, 2011, **133**, 2816-2819.
87. J. Wang, M. Zhu, R. A. Outlaw, X. Zhao, D. M. Manos and B. C. Holloway, *Carbon*, 2004, **42**, 2867-2872.
88. J. J. Wang, M. Y. Zhu, R. A. Outlaw, X. Zhao, D. M. Manos, B. C. Holloway and V. P. Mammana, *Free-standing subnanometer graphite sheets*, AIP, 2004.

89. A. Malesevic, R. Vitchev, K. Schouteden, A. Volodin, L. Zhang, G. V. Tendeloo, A. Vanhulsel and C. V. Haesendonck, *Nanotechnology*, 2008, **19**, 305604.
90. R. Vitchev, A. Malesevic, R. H. Petrov, R. Kemps, M. Mertens, A. Vanhulsel and C. Van Haesendonck, *Nanotechnology*, 2010, **21**, 095602.
91. M. Zhu, J. Wang, B. C. Holloway, R. A. Outlaw, X. Zhao, K. Hou, V. Shutthanandan and D. M. Manos, *Carbon*, 2007, **45**, 2229-2234.
92. S. Hagstrom, H. B. Lyon and G. A. Somorjai, *Physical Review Letters*, 1965, **15**, 491.
93. H. Lyon and G. Somorjai, *The Journal of Chemical Physics*, 1967, **46**, 2539.
94. J. T. Grant and T. W. Haas, *Surface Science*, 1970, **21**, 76-85.
95. L. C. Isett and J. M. Blakely, *Surface Science*, 1976, **58**, 397-414.
96. Y. Gamo, A. Nagashima, M. Wakabayashi, M. Terai and C. Oshima, *Surface Science*, 1997, **374**, 61-64.
97. D. G. Castner, B. A. Sexton and G. A. Somorjai, *Surface Science*, 1978, **71**, 519-540.
98. B. Lang, *Surface Science*, 1975, **53**, 317-329.
99. B. E. Nieuwenhuys, D. I. Hagen, G. Rovida and G. A. Somorjai, *Surface Science*, 1976, **59**, 155-176.
100. K. Baron, D. W. Blakely and G. A. Somorjai, *Surface Science*, 1974, **41**, 45-66.
101. P. Sutter, M. S. Hybertsen, J. T. Sadowski and E. Sutter, *Nano Letters*, 2009, **9**, 2654-2660.
102. E. Moreau, F. J. Ferrer, D. Vignaud, S. Godey and X. Wallart, *physica status solidi (a)*, 2010, **207**, 300-303.
103. R. Nair, P. Blake, A. Grigorenko, K. Novoselov, T. Booth, T. Stauber, N. Peres and A. Geim, *Science*, 2008, **320**, 1308.
104. K. F. Mak, M. Y. Sfeir, Y. Wu, C. H. Lui, J. A. Misewich and T. F. Heinz, *Physical Review Letters*, 2008, **101**, 196405.
105. A. Lambacher and P. Fromherz, *Applied Physics A: Materials Science & Processing*, 1996, **63**, 207-216.
106. D. Abergel, A. Russell and V. I. Fal'ko, *Applied Physics Letters*, 2007, **91**, 063125.
107. P. Blake, E. Hill, A. H. C. Neto, K. Novoselov, D. Jiang, R. Yang, T. Booth and A. Geim, *Applied Physics Letters*, 2007, **91**, 063124.
108. L. Gao, W. Ren, F. Li and H.-M. Cheng, *ACS Nano*, 2008, **2**, 1625-1633.
109. I. Jung, M. Pelton, R. Piner, D. A. Dikin, S. Stankovich, S. Watcharotone, M. Hausner and R. S. Ruoff, *Nano Letters*, 2007, **7**, 3569-3575.
110. I. Jung, R. Piner, D. Dikin, S. Stankovich, R. S. Ruoff and M. Hausner, *Bulletin of the American Physical Society*, 2006.
111. S. Roddaro, P. Pingue, V. Piazza, V. Pellegrini and F. Beltram, *Nano Letters*, 2007, **7**, 2707-2710.
112. G. Rietveld, H. van Elferen, A. Giesbers, A. Veligura, U. Zeitler, K. Novoselov, B. van Wees, A. Geim and J. Maan, IEEE, pp. 627-628.
113. J. Weber, V. Calado and M. van de Sanden, *Applied Physics Letters*, 2010, **97**, 091904.
114. U. Wurstbauer, C. Röling, W. Wegscheider, M. Vaupel, P. H. Thiesen and D. Weiss, *Applied Physics Letters*, 2010, **97**, 231901.
115. C. Casiraghi, A. Hartschuh, E. Lidorikis, H. Qian, H. Harutyunyan, T. Gokus, K. S. Novoselov and A. C. Ferrari, *Nano Letters*, 2007, **7**, 2711-2717.
116. J. Kim, L. J. Cote, F. Kim and J. Huang, *Journal of the American Chemical Society*, 2009, **132**, 260-267.
117. E. Treossi, M. Melucci, A. Liscio, M. Gazzano, P. Samorì and V. Palermo, *Journal of the American Chemical Society*, 2009, **131**, 15576-15577.
118. A. Gray, M. Balooch, S. Allegret, S. De Gendt and W. E. Wang, *Journal of Applied Physics*, 2008, **104**, 053109-053109-053108.
119. Q. Zhan and J. R. Leger, *Applied optics*, 2002, **41**, 4443-4450.

120. M. Y. Sfeir, T. Beetz, F. Wang, L. Huang, X. M. H. Huang, M. Huang, J. Hone, S. O'Brien, J. A. Misewich, T. F. Heinz, L. Wu, Y. Zhu and L. E. Brus, *Science*, 2006, **312**, 554-556.
121. F. Wang, M. Y. Sfeir, L. Huang, X. M. H. Huang, Y. Wu, J. Kim, J. Hone, S. O'Brien, L. E. Brus and T. F. Heinz, *Physical Review Letters*, 2006, **96**, 167401.
122. E. Stolyarova, K. T. Rim, S. Ryu, J. Maultzsch, P. Kim, L. E. Brus, T. F. Heinz, M. S. Hybertsen and G. W. Flynn, *Proceedings of the National Academy of Sciences*, 2007, **104**, 9209.
123. P. Lauffer, K. V. Emtsev, R. Graupner, T. Seyller, L. Ley, S. A. Reshanov and H. B. Weber, *Physical Review B*, 2008, **77**, 155426.
124. J. I. Paredes, S. Villar-Rodil, P. Solís-Fernández, A. Martínez-Alonso and J. M. D. Tascón, *Langmuir*, 2009, **25**, 5957-5968.
125. C. Lee, X. Wei, J. W. Kysar and J. Hone, *Science*, 2008, **321**, 385.
126. C. Lee, X. Wei, Q. Li, R. Carpick, J. W. Kysar and J. Hone, *physica status solidi (b)*, 2009, **246**, 2562-2567.
127. R. J. Nemanich and S. A. Solin, *Physical Review B*, 1979, **20**, 392.
128. A. C. Ferrari and J. Robertson, *Physical Review B*, 2000, **61**, 14095.
129. A. C. Ferrari, *Solid State Communications*, 2007, **143**, 47-57.
130. C. Casiraghi, *Physical Review B*, 2009, **80**, 233407.
131. A. Das, B. Chakraborty and A. Sood, *Bulletin of Materials Science*, 2008, **31**, 579-584.
132. A. Jorio, E. H. M. Ferreira, M. V. O. Moutinho, F. Stavale, C. A. Achete and R. B. Capaz, *physica status solidi (b)*, 2010, **247**, 2980-2982.
133. M. Pimenta, G. Dresselhaus, M. S. Dresselhaus, L. Cancado, A. Jorio and R. Saito, *Phys. Chem. Chem. Phys.*, 2007, **9**, 1276-1290.
134. C. Casiraghi, S. Pisana, K. Novoselov, A. Geim and A. Ferrari, *Applied Physics Letters*, 2007, **91**, 233108.
135. Y. M. You, Z. H. Ni, T. Yu and Z. X. Shen, *Applied Physics Letters*, 2008, **93**, 163112.
136. T. M. G. Mohiuddin, A. Lombardo, R. R. Nair, A. Bonetti, G. Savini, R. Jalil, N. Bonini, D. M. Basko, C. Galiotis, N. Marzari, K. S. Novoselov, A. K. Geim and A. C. Ferrari, *Physical Review B*, 2009, **79**, 205433.
137. A. A. Balandin, S. Ghosh, W. Bao, I. Calizo, D. Teweldebrhan, F. Miao and C. N. Lau, *Nano Letters*, 2008, **8**, 902-907.
138. A. Ferrari, J. Meyer, V. Scardaci, C. Casiraghi, M. Lazzeri, F. Mauri, S. Piscanec, D. Jiang, K. Novoselov and S. Roth, *Physical Review Letters*, 2006, **97**, 187401.
139. A. Gupta, G. Chen, P. Joshi, S. Tadigadapa and Eklund, *Nano Letters*, 2006, **6**, 2667-2673.
140. D. Graf, F. Molitor, K. Ensslin, C. Stampfer, A. Jungen, C. Hierold and L. Wirtz, *Nano Letters*, 2007, **7**, 238-242.
141. R. John, A. Ashokreddy, C. Vijayan and T. Pradeep, *Nanotechnology*, 2011, **22**, 165701.
142. I. Calizo, W. Bao, F. Miao, C. N. Lau and A. A. Balandin, *Applied Physics Letters*, 2007, **91**, 201904-201904-201903.
143. M. Xu, D. Fujita, J. Gao and N. Hanagata, *ACS Nano*, 2010, **4**, 2937-2945.
144. H. Kawanowa, H. Ozawa, T. Yazaki, Y. Gotoh and R. Souda, *Jpn. J. Appl. Phys*, 2002, **41**, 6149-6152.
145. A. M. Shikin, G. V. Prudnikova, V. K. Adamchuk, F. Moresco and K. H. Rieder, *Physical Review B*, 2000, **62**, 13202.
146. T. Aizawa, R. Souda, Y. Ishizawa, H. Hirano, T. Yamada, K.-i. Tanaka and C. Oshima, *Surface Science*, 1990, **237**, 194-202.
147. A. M. Shikin, D. FarIas, V. K. Adamchuk and K. H. Rieder, *Surface Science*, 1999, **424**, 155-167.
148. A. Shikin, D. Farias and K. Rieder, *EPL (Europhysics Letters)*, 1998, **44**, 44.
149. D. Farias, A. Shikin, K. Rieder and Y. S. Dedkov, *Journal of Physics: Condensed Matter*, 1999, **11**, 8453.

150. D. Farías, K. H. Rieder, A. M. Shikin, V. K. Adamchuk, T. Tanaka and C. Oshima, *Surface Science*, 2000, **454**, 437-441.
151. T. Aizawa, Y. Hwang, W. Hayami, R. Souda, S. Otani and Y. Ishizawa, *Surface Science*, 1992, **260**, 311-318.
152. H. Yanagisawa, T. Tanaka, Y. Ishida, M. Matsue, E. Rokuta, S. Otani and C. Oshima, *Surface and Interface Analysis*, 2005, **37**, 133-136.
153. R. J. Koch, T. Haensel, S. I. U. Ahmed, T. Seyller and J. A. Schaefer, *physica status solidi (c)*, 2010, **7**, 394-397.
154. D. Wei, Y. Liu, Y. Wang, H. Zhang, L. Huang and G. Yu, *Nano Letters*, 2009, **9**, 1752-1758.
155. A. Bostwick, T. Ohta, T. Seyller, K. Horn and E. Rotenberg, *Nat Phys*, 2007, **3**, 36-40.
156. S. Y. Zhou, D. A. Siegel, A. V. Fedorov, F. E. Gabaly, A. K. Schmid, A. H. C. Neto, D. H. Lee and A. Lanzara, *Nat Mater*, 2008, **7**, 259-260.
157. A. H. Castro Neto, F. Guinea, N. M. R. Peres, K. S. Novoselov and A. K. Geim, *Reviews of Modern Physics*, 2009, **81**, 109.
158. N. Staley, H. Wang, C. Puls, J. Forster, T. N. Jackson, K. McCarthy, B. Clouser and Y. Liu, *Lithography-free fabrication of graphene devices*, AIP, 2007.
159. G. Eda and M. Chhowalla, *Nano Letters*, 2009, **9**, 814-818.
160. L. Liao, J. Bai, R. Cheng, H. Zhou, L. Liu, Y. Liu, Y. Huang and X. Duan, *Nano Letters*, 2011, null-null.
161. L. Yu-Ming, C. Hsin-Ying, K. A. Jenkins, D. B. Farmer, P. Avouris and A. Valdes-Garcia, *Electron Device Letters, IEEE*, 2010, **31**, 68-70.
162. Y.-M. Lin, K. A. Jenkins, A. Valdes-Garcia, J. P. Small, D. B. Farmer and P. Avouris, *Nano Letters*, 2008, **9**, 422-426.
163. Y. Wu, Y.-m. Lin, A. A. Bol, K. A. Jenkins, F. Xia, D. B. Farmer, Y. Zhu and P. Avouris, *Nature*, 2011, **472**, 74-78.
164. Y.-M. Lin, C. Dimitrakopoulos, K. A. Jenkins, D. B. Farmer, H.-Y. Chiu, A. Grill and P. Avouris, *Science*, 2010, **327**, 662.
165. Z. Chen, Y.-M. Lin, M. J. Rooks and P. Avouris, *Physica E: Low-dimensional Systems and Nanostructures*, 2007, **40**, 228-232.
166. F. Rana, *Nanotechnology, IEEE Transactions on*, 2008, **7**, 91-99.
167. F. Rana, J. H. Strait, P. A. George, H. Wang and J. D. Besant, IEEE, pp. 650-651.
168. Q. Bao, H. Zhang, Y. Wang, Z. Ni, Y. Yan, Z. X. Shen, K. P. Loh and D. Y. Tang, *Advanced Functional Materials*, 2009, **19**, 3077-3083.
169. F. Bonaccorso, Z. Sun, T. Hasan and A. Ferrari, *Nature Photonics*, 2010, **4**, 611-622.
170. H. Zhang, D. Tang, L. Zhao, Q. Bao and K. Loh, *Arxiv preprint arXiv:0909.5536*, 2009.
171. H. Zhang, D. Tang, R. Knize, L. Zhao, Q. Bao and K. P. Loh, *Applied Physics Letters*, 2010, **96**, 111112.
172. W. B. Cho, H. W. Lee, S. Y. Choi, J. W. Kim, D. I. Yeom, F. Rotermund, J. Kim and B. H. Hong, Optical Society of America, 2010.
173. C. C. Lee, G. Acosta, J. Bunch and T. Schibli, *Arxiv preprint arXiv:1010.0990*, 2010.
174. Z. Sun, T. Hasan, F. Torrisi, D. Popa, G. Privitera, F. Wang, F. Bonaccorso, D. M. Basko and A. C. Ferrari, *ACS Nano*, 2010, **4**, 803-810.
175. T. Hasan, Z. Sun, F. Wang, F. Bonaccorso, P. H. Tan, A. G. Rozhin and A. C. Ferrari, *Advanced Materials*, 2009, **21**, 3874-3899.
176. H. Zhang, Q. Bao, D. Tang, L. Zhao and K. Loh, *Applied Physics Letters*, 2009, **95**, 141103.
177. T. Hasan, Z. Sun, F. Wang, F. Bonaccorso, P. H. Tan, A. G. Rozhin and A. C. Ferrari, *Advanced Materials*, 2009, **21**, 3874-3899.
178. Z. Sun, D. Popa, T. Hasan, F. Torrisi, F. Wang, E. J. R. Kelleher, J. C. Travers, V. Nicolosi and A. C. Ferrari, *Nano Research*, 2010, **3**, 653-660.
179. Y. W. Song, S. Y. Jang, W. S. Han and M. K. Bae, *Applied Physics Letters*, 2010, **96**, 051122.

180. W. Tan, C. Su, R. Knize, G. Xie, L. Li and D. Tang, *Applied Physics Letters*, 2010, **96**, 031106-031106-031103.
181. A. Candini, S. Klyatskaya, M. Ruben, W. Wernsdorfer and M. Affronte, *Nano Letters*, 2011, **11**, 2634-2639.
182. Q. Zhang, K. S. Chan and Z. Lin, *Spin current generation by adiabatic pumping in monolayer graphene*, AIP, 2011.
183. D. Gunlycke, D. A. Areshkin, J. Li, J. W. Mintmire and C. T. White, *Nano Letters*, 2007, **7**, 3608-3611.
184. J.-H. Chen, L. Li, W. G. Cullen, E. D. Williams and M. S. Fuhrer, *Nat Phys*, 2011, **7**, 535-538.
185. T. S. Jespersen, K. Grove-Rasmussen, J. Paaske, K. Muraki, T. Fujisawa, J. Nygard and K. Flensberg, *Nat Phys*, 2011, **7**, 348-353.
186. I. Zaliznyak, A. Tsvelik and D. Kharzeev, Google Patents, 2013.
187. Y.-W. Son, M. L. Cohen and S. G. Louie, *Nature*, 2006, **444**, 347-349.
188. L. Brey, H. A. Fertig and S. Das Sarma, *Physical Review Letters*, 2007, **99**, 116802.
189. M. Wimmer, İ. Adagideli, S. Berber, D. Tománek and K. Richter, *Physical Review Letters*, 2008, **100**, 177207.
190. N. Tombros, C. Jozsa, M. Popinciuc, H. T. Jonkman and B. J. van Wees, *Nature*, 2007, **448**, 571-574.
191. V. Fal'ko, *Nat Phys*, 2007, **3**, 151-152.
192. B. Trauzettel, D. V. Bulaev, D. Loss and G. Burkard, *Nat Phys*, 2007, **3**, 192-196.
193. V. Gupta, N. Chaudhary, R. Srivastava, G. D. Sharma, R. Bhardwaj and S. Chand, *Journal of the American Chemical Society*, 2011, **133**, 9960-9963.
194. S. Bae, H. Kim, Y. Lee, X. Xu, J. S. Park, Y. Zheng, J. Balakrishnan, T. Lei, H. R. Kim and Y. I. Song, *Nature Nanotechnology*, 2010, **5**, 574-578.
195. G. Eda, H. E. Unalan, N. Rupesinghe, G. A. J. Amaratunga and M. Chhowalla, *Applied Physics Letters*, 2008, **93**, 233502.
196. Z. S. Wu, S. Pei, W. Ren, D. Tang, L. Gao, B. Liu, F. Li, C. Liu and H. M. Cheng, *Advanced Materials*, 2009, **21**, 1756-1760.
197. I. Lahiri, V. P. Verma and W. Choi, *Carbon*, 2011, **49**, 1614-1619.
198. A. Malesevic, R. Kemps, A. Vanhulsel, M. P. Chowdhury, A. Volodin and C. Van Haesendonck, *Journal of Applied Physics*, 2008, **104**, 084301-084301-084305.
199. N. Papasimakis, Z. Luo, Z. X. Shen, F. De Angelis, E. Di Fabrizio, A. E. Nikolaenko and N. I. Zheludev, *Opt. Express*, 2010, **18**, 8353–8359.
200. Q. Zheng, W. H. Ip, X. Lin, N. Yousefi, K. K. Yeung, Z. Li and J.-K. Kim, *ACS Nano*, 2011.
201. J. Kim, M. Ishihara, Y. Koga, K. Tsugawa, M. Hasegawa and S. Iijima, *Low-temperature synthesis of large-area graphene-based transparent conductive films using surface wave plasma chemical vapor deposition*, AIP, 2011.
202. Y. Zhu, Z. Sun, Z. Yan, Z. Jin and J. M. Tour, *ACS Nano*, 2011, null-null.
203. Y. Si and E. T. Samulski, *Chemistry of Materials*, 2008, **20**, 6792-6797.
204. B. Seger and P. V. Kamat, *The Journal of Physical Chemistry C*, 2009, **113**, 7990-7995.
205. R. Kou, Y. Shao, D. Wang, M. H. Engelhard, J. H. Kwak, J. Wang, V. V. Viswanathan, C. Wang, Y. Lin and Y. Wang, *Electrochemistry Communications*, 2009, **11**, 954-957.
206. E. Yoo, T. Okata, T. Akita, M. Kohyama, J. Nakamura and I. Honma, *Nano Letters*, 2009, **9**, 2255-2259.
207. Y. Li, L. Tang and J. Li, *Electrochemistry Communications*, 2009, **11**, 846-849.
208. L. Qu, Y. Liu, J.-B. Baek and L. Dai, *ACS Nano*, 2010, **4**, 1321-1326.
209. X. Wang, L. Zhi and K. Müllen, *Nano Letters*, 2008, **8**, 323-327.
210. X. Wang, L. Zhi, N. Tsao, Ž. Tomović, J. Li and K. Müllen, *Angewandte Chemie International Edition*, 2008, **47**, 2990-2992.
211. J. Wu, H. A. Becerril, Z. Bao, Z. Liu, Y. Chen and P. Peumans, *Applied Physics Letters*, 2008, **92**, 263302.

212. Y. Wang, X. Chen, Y. Zhong, F. Zhu and K. P. Loh, *Applied Physics Letters*, 2009, **95**, 063302.
213. X. Yan, X. Cui, B. Li and L.-s. Li, *Nano Letters*, 2010, **10**, 1869-1873.
214. B. E. Conway, *Electrochemical supercapacitors: scientific fundamentals and technological applications*, Springer, 1999.
215. M. D. Stoller, S. Park, Y. Zhu, J. An and R. S. Ruoff, *Nano Letters*, 2008, **8**, 3498-3502.
216. L. L. Zhang, R. Zhou and X. Zhao, *J. Mater. Chem.*, 2010, **20**, 5983-5992.
217. K. Zhang, L. L. Zhang, X. S. Zhao and J. Wu, *Chemistry of Materials*, 2010, **22**, 1392-1401.
218. X. Yang, J. Zhu, L. Qiu and D. Li, *Advanced Materials*, 2011, **23**, 2833-2838.
219. K.-S. Kim, H.-J. Lee, C. Lee, S.-K. Lee, H. Jang, J.-H. Ahn, J.-H. Kim and H.-J. Lee, *ACS Nano*, 2011.
220. G. K. Dimitrakakis, E. Tylianakis and G. E. Froudakis, *Nano Letters*, 2008, **8**, 3166-3170.
221. T. Takamura, K. Endo, L. Fu, Y. Wu, K. J. Lee and T. Matsumoto, *Electrochimica Acta*, 2007, **53**, 1055-1061.
222. E. Yoo, J. Kim, E. Hosono, H.-s. Zhou, T. Kudo and I. Honma, *Nano Letters*, 2008, **8**, 2277-2282.
223. D. Wang, D. Choi, J. Li, Z. Yang, Z. Nie, R. Kou, D. Hu, C. Wang, L. V. Saraf, J. Zhang, I. A. Aksay and J. Liu, *ACS Nano*, 2009, **3**, 907-914.
224. L. Ji, Z. Tan, T. Kuykendall, E. J. An, Y. Fu, V. Battaglia and Y. Zhang, *Energy & Environmental Science*, 2011.
225. H. Gwon, H. S. Kim, K. U. Lee, D. H. Seo, Y. C. Park, Y. S. Lee, B. T. Ahn and K. Kang, *Energy Environ. Sci.*, 2011.
226. Z. Chen, W. Ren, L. Gao, B. Liu, S. Pei and H.-M. Cheng, *Nat Mater*, 2011, **10**, 424-428.
227. S. N. Baker and G. A. Baker, *Angewandte Chemie International Edition*, 2010, **49**, 6726-6744.
228. S. Zhu, J. Zhang, C. Qiao, S. Tang, Y. Li, W. Yuan, B. Li, L. Tian, F. Liu and R. Hu, *Chem. Commun.*, 2011, **47**, 6858-6860.
229. Y. Wang, H. B. Yao, X. H. Wang and S. H. Yu, *J. Mater. Chem.*, 2010.
230. F. Schedin, A. K. Geim, S. V. Morozov, E. W. Hill, P. Blake, M. I. Katsnelson and K. S. Novoselov, *Nat Mater*, 2007, **6**, 652-655.
231. J. T. Robinson, F. K. Perkins, E. S. Snow, Z. Wei and P. E. Sheehan, *Nano Letters*, 2008, **8**, 3137-3140.
232. J. D. Fowler, M. J. Allen, V. C. Tung, Y. Yang, R. B. Kaner and B. H. Weiller, *ACS Nano*, 2009, **3**, 301-306.
233. Y. Lu, B. R. Goldsmith, N. J. Kybert and A. T. C. Johnson, *DNA-decorated graphene chemical sensors*, AIP, 2010.
234. J. L. Johnson, A. Behnam, S. J. Pearton and A. Ural, *Advanced Materials*, 2010, **22**, 4877-4880.
235. Y. Dan, Y. Lu, N. J. Kybert, Z. Luo and A. T. C. Johnson, *Nano Letters*, 2009, **9**, 1472-1475.
236. C. Shan, H. Yang, J. Song, D. Han, A. Ivaska and L. Niu, *Analytical Chemistry*, 2009, **81**, 2378-2382.
237. J. Lu, L. T. Drzal, R. M. Worden and I. Lee, *Chemistry of Materials*, 2007, **19**, 6240-6246.
238. V. Chandra, J. Park, Y. Chun, J. W. Lee, I.-C. Hwang and K. S. Kim, *ACS Nano*, 2010, **4**, 3979-3986.
239. G. Wei, Y.-E. Miao, C. Zhang, Z. Yang, Z. Liu, W. W. Tjiu and T. Liu, *ACS Applied Materials & Interfaces*, 2013, **5**, 7584-7591.
240. Y. Liu, J. Ma, T. Wu, X. Wang, G. Huang, Y. Liu, H. Qiu, Y. Li, W. Wang and J. Gao, *ACS Applied Materials & Interfaces*, 2013, **5**, 10018-10026.
241. H. Chen, M. B. Müller, K. J. Gilmore, G. G. Wallace and D. Li, *Advanced Materials*, 2008, **20**, 3557-3561.
242. C. Wang, D. Li, C. O. Too and G. G. Wallace, *Chemistry of Materials*, 2009, **21**, 2604-2606.
243. J. K. Lee, K. B. Smith, C. M. Hayner and H. H. Kung, *Chem. Commun.*, 2010, **46**, 2025-2027.

244. E. Stolyarova, D. Stolyarov, K. Bolotin, S. Ryu, L. Liu, K. T. Rim, M. Klima, M. Hybertsen, I. Pogorelsky, I. Pavlishin, K. Kusche, J. Hone, P. Kim, H. L. Stormer, V. Yakimenko and G. Flynn, *Nano Letters*, 2008, **9**, 332-337.
245. D.-e. Jiang, V. R. Cooper and S. Dai, *Nano Letters*, 2009, **9**, 4019-4024.
246. T. V. Duncan, *Journal of Colloid and Interface Science*, **In Press, Corrected Proof**.
247. M. F. Yu, B. S. Files, S. Arepalli and R. S. Ruoff, *Physical Review Letters*, 2000, **84**, 5552-5555.
248. E. W. Wong, P. E. Sheehan and C. M. Lieber, *Science*, 1997, **277**, 1971.
249. M. Fujii, X. Zhang and K. Takahashi, *physica status solidi (b)*, 2006, **243**, 3385-3389.
250. C. Yu, L. Shi, Z. Yao, D. Li and A. Majumdar, *Nano Letters*, 2005, **5**, 1842-1846.
251. S. Berber, Y. K. Kwon and D. Tománek, *Physical Review Letters*, 2000, **84**, 4613-4616.
252. P. Kim, L. Shi, A. Majumdar and P. McEuen, *Physical Review Letters*, 2001, **87**, 215502.
253. M. Freitag, M. Steiner, Y. Martin, V. Perebeinos, Z. Chen, J. C. Tsang and P. Avouris, *Nano Letters*, 2009, **9**, 1883-1888.
254. F. Miao, S. Wijeratne, Y. Zhang, U. Coskun, W. Bao and C. Lau, *Science*, 2007, **317**, 1530.
255. X. Du, I. Skachko, A. Barker and E. Y. Andrei, *Nat Nano*, 2008, **3**, 491-495.
256. R. Murali, Y. Yang, K. Brenner, T. Beck and J. D. Meindl, *Breakdown current density of graphene nanoribbons*, AIP, 2009.
257. Y. Tianhua, L. Eun-Kyu, B. Briggs, B. Nagabhirava and Y. Bin, *Electron Device Letters, IEEE*, 2010, **31**, 1155-1157.
258. M. Dragoman and D. Dragoman, *Progress in Quantum Electronics*, 2009, **33**, 165-214.
259. Z. Y. Ong and E. Pop, *PHYSICAL REVIEW B Phys Rev B*, 2010, **81**, 155408.
260. A. Peigney, C. Laurent, E. Flahaut, R. R. Bacsa and A. Rousset, *Carbon*, 2001, **39**, 507-514.
261. T. Hiraoka, A. Izadi-Najafabadi, T. Yamada, D. N. Futaba, S. Yasuda, O. Tanaike, H. Hatori, M. Yumura, S. Iijima and K. Hata, *Advanced Functional Materials*, 2010, **20**, 422-428.
262. C. Trottier, *Journal of the SID*, 2005, 759.
263. A. Fujiwara, K. Tomiyama, H. Suematsu, M. Yumura and K. Uchida, *Physical Review B*, 1999, **60**, 13492.
264. L. E. Hueso, J. M. Pruneda, V. Ferrari, G. Burnell, J. P. Valdes-Herrera, B. D. Simons, P. B. Littlewood, E. Artacho, A. Fert and N. D. Mathur, *Nature*, 2007, **445**, 410-413.
265. Y. Zhao, A. Liao and E. Pop, *Electron Device Letters, IEEE*, 2009, **30**, 1078-1080.
266. T. Dürkop, B. Kim and M. Fuhrer, *Journal of Physics: Condensed Matter*, 2004, **16**, R553.
267. S. Hong and S. Myung, *Nat Nano*, 2007, **2**, 207-208.
268. P. Jarillo-Herrero, J. A. van Dam and L. P. Kouwenhoven, *Nature*, 2006, **439**, 953-956.

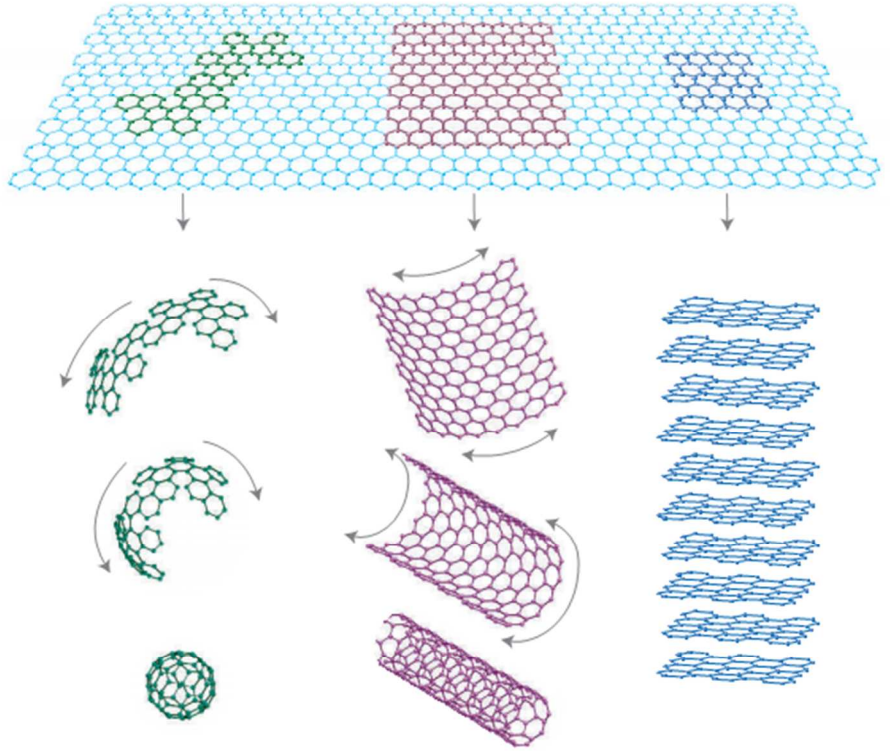

Figure 1. Graphene - the source of graphitic nanomaterials of 0D, 1D and 3D dimensions. Reprinted with permission from ref. 12.

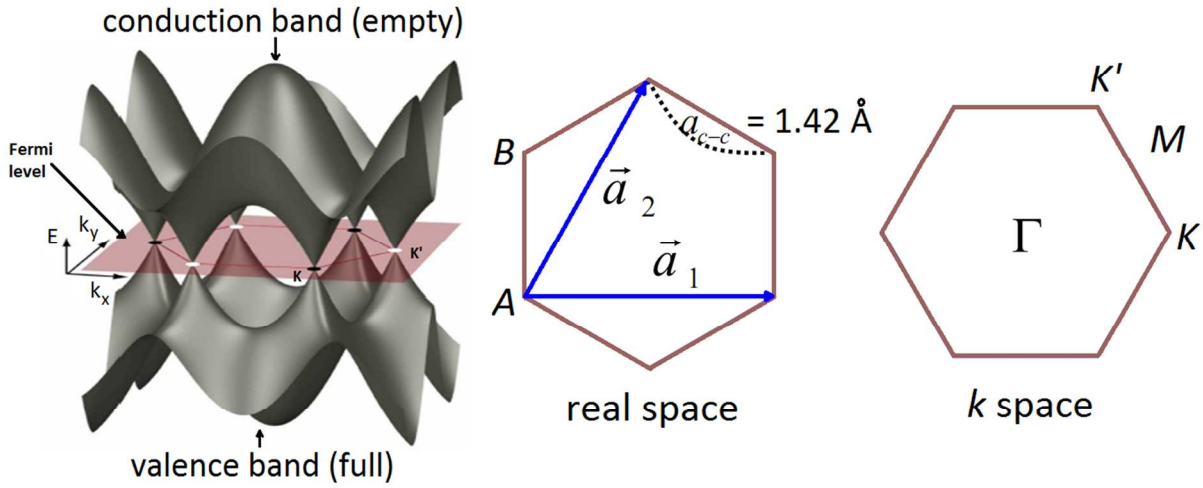

Figure 2. Dirac cone arrangement (Electronic band structure) in real space and in *k*-space. Reprinted with permission from ref. 13

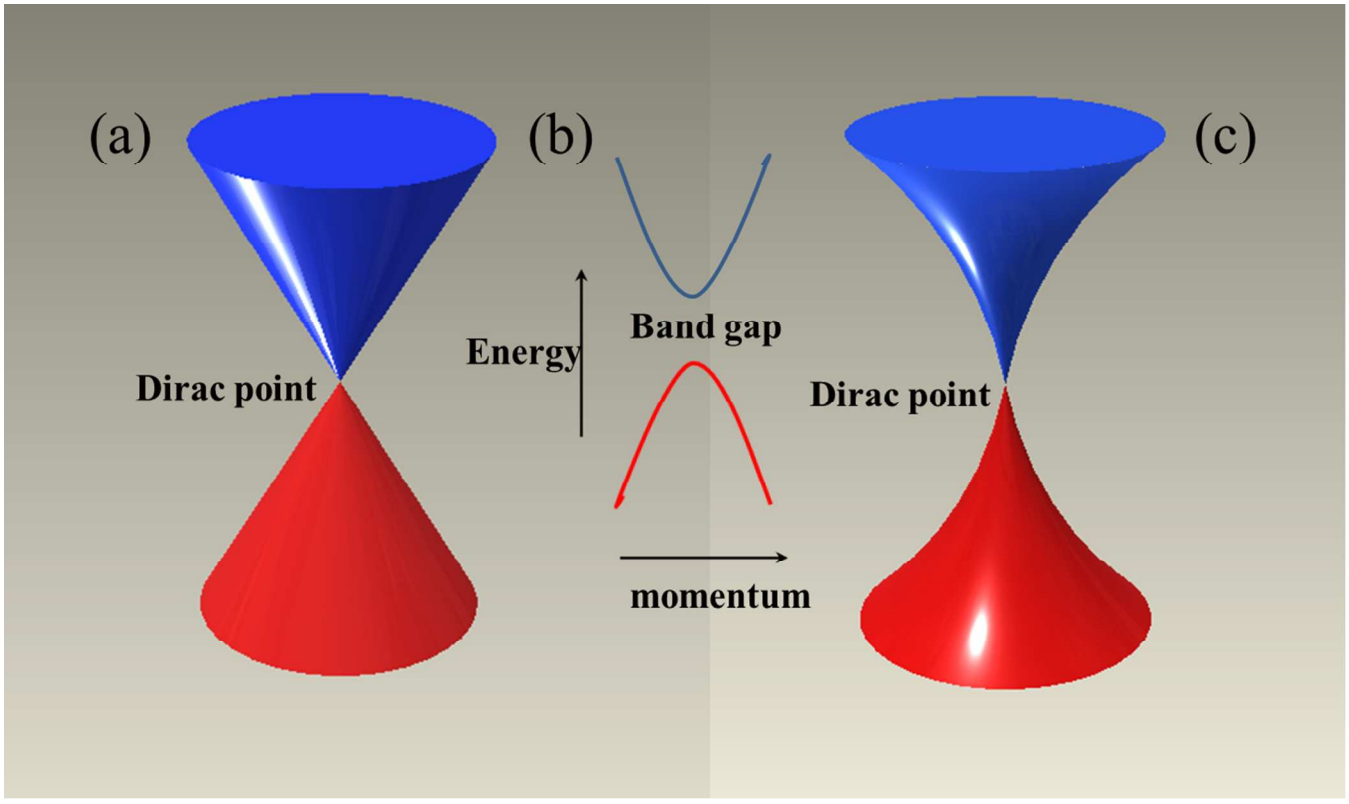

Figure 3. The energy bands of two-dimensional graphene (a) are smooth-sided cones, which meet at the Dirac point. The band structure of a conventional three-dimensional material (b) is parabolic, with a band gap between the lower-energy valence band and the higher-energy conduction band. The ARPES spectrum of undoped graphene (c) exhibiting a distinct inward curvature

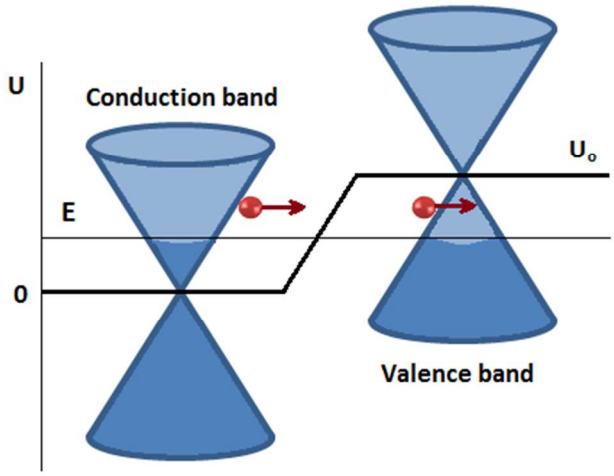

Figure 4. Klein Paradox effect.

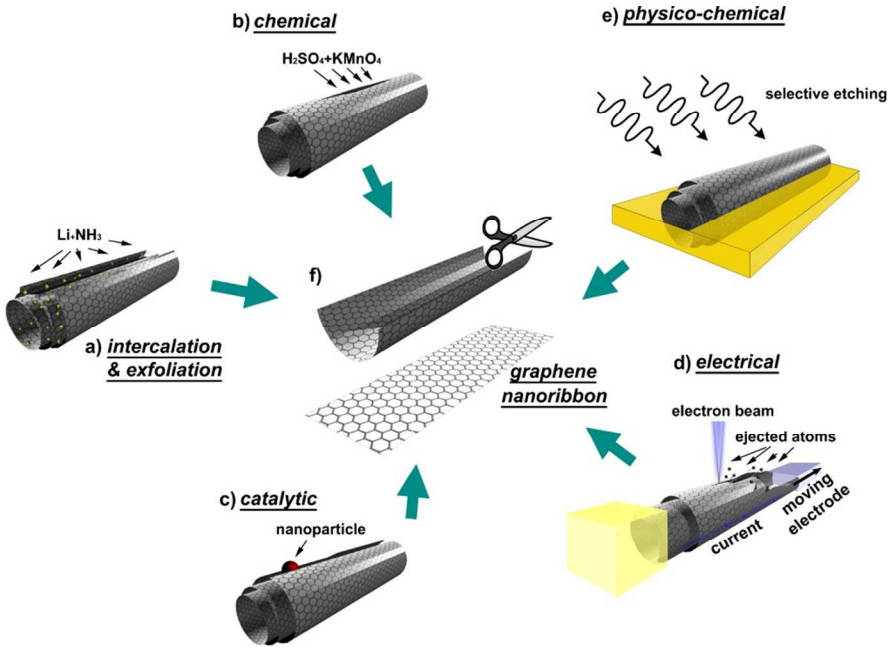

Figure 5. Illustration of unzipping of CNTs to form Graphene Nanoribbons. Reprinted with permission from ref. 55.

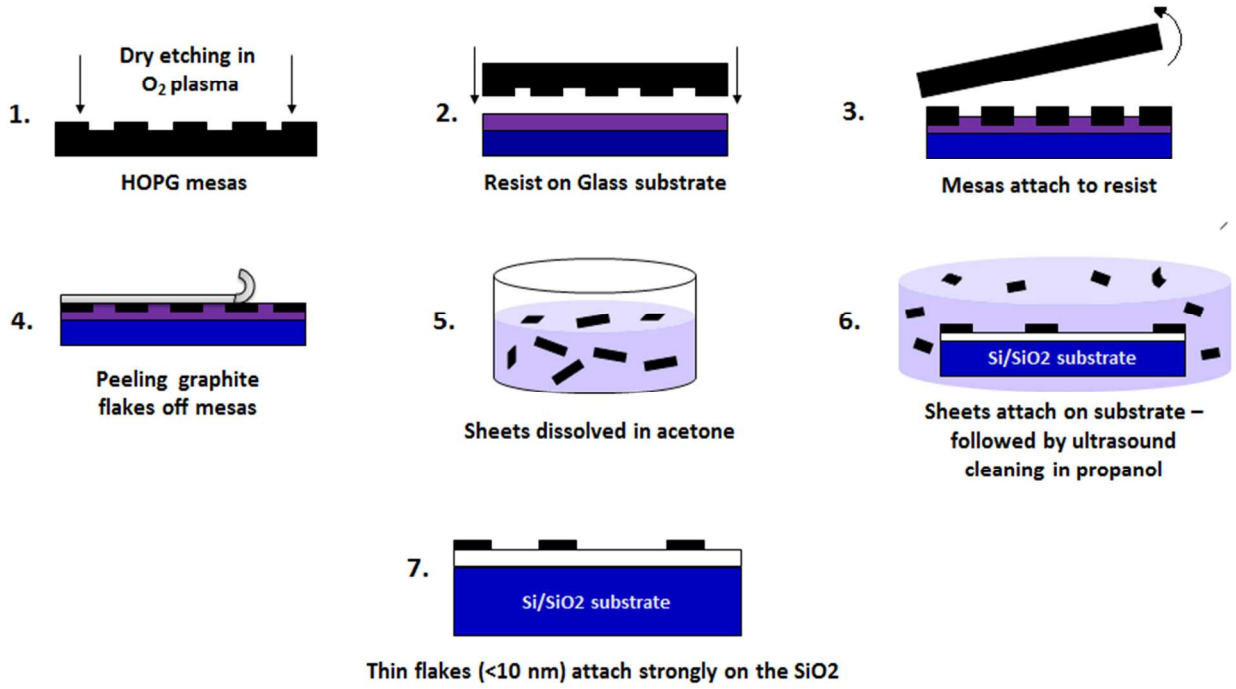

Figure 6. Exfoliation of graphite and attachment of thin graphene flakes on Si/SiO_2 substrate. Reprinted with permission from ref. 15.

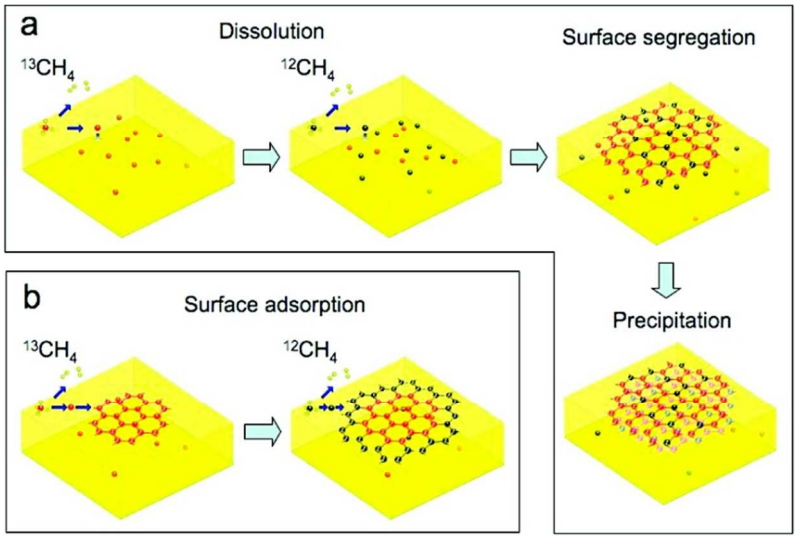

Figure 7. Graphenization Mechanism for (a) Ni and (b) Cu. Reprinted with permission from ref. 81.

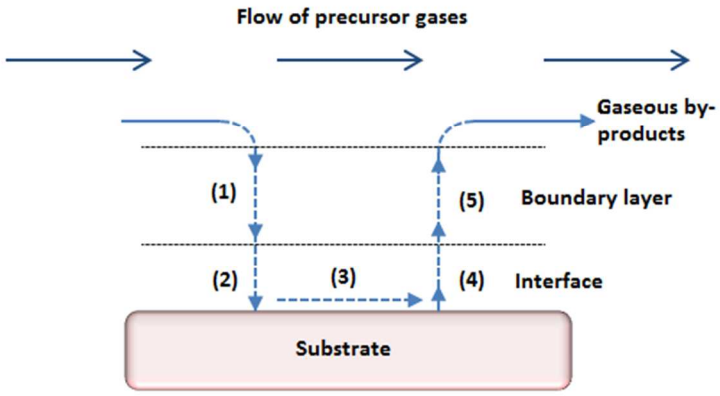

Figure 8. Kinetics of CVD process

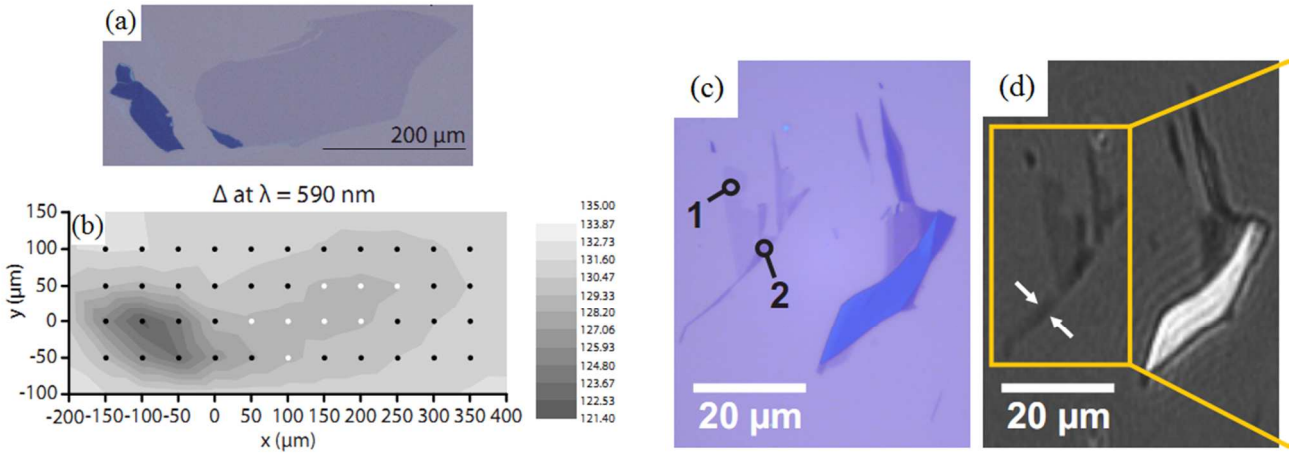

Figure 9. (a) An optical image exposed to visible light, showing Multi-layer Graphene (dark blue). (b) Spectroscopic ellipsometric scan of the map – white dots indicating the spectra that can be attributed to originate from graphene only. The shape enclosing the white dots also resembles the shape of the real flake. (Optical constants of graphene measured by spectroscopic ellipsometry). Reprinted with permission from ref. 113. (c) Optical image and (d) imaging ellipsometric intensity image of a sample on SiO_2/Si showing regions with graphene monolayer covering up to thin graphite. Numbers in (d) correspond to the layer numbers – Wurstba – Imaging ellipsometry of graphene. Reprinted with permission from ref. 114.

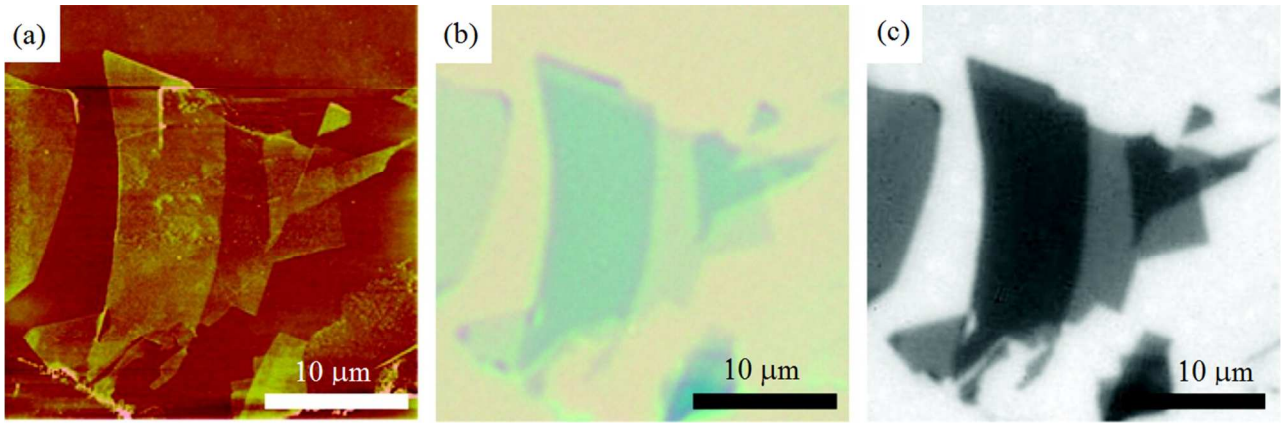

Figure 10. Mechanically exfoliated graphene on a SiO2/Si substrate taken by (a) AFM, (b) optical microscopy, (c) FQM using PVP/fluorescein. Reprinted with permission from ref. 116.

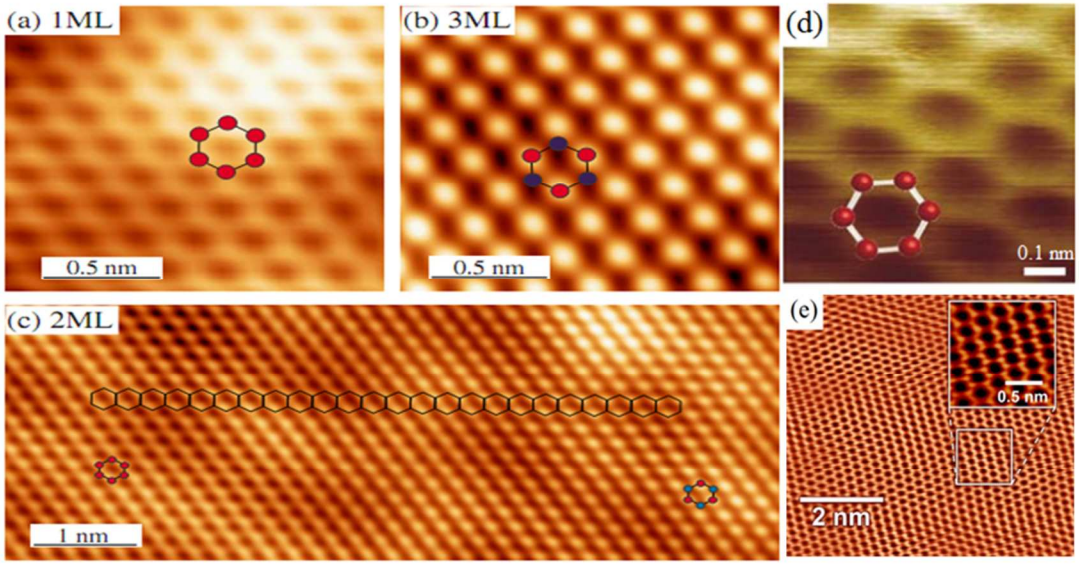

Figure 11. Atomic resolution STM image of (a) Single Layer graphene (b) Tri-layer graphene and (c) Bi-layer graphene. The honeycomb structure of graphene is indicated by hexagons showing equivalent atoms for a monolayer case and inequivalent atoms for the tri-layer case and part of the bi-layer case. Reprinted with permission from ref. 123. Atomic and electronic structure of few-layer graphene on SiC(0001) studied with scanning tunneling microscopy and spectroscopy) (d) High resolution STM image of a mesoscopic graphene sheet. (e) Atomic resolution STM Image of a graphite structure (zoomed portion shows the honeycomb lattice structure). Reprinted with permission from ref. 122.

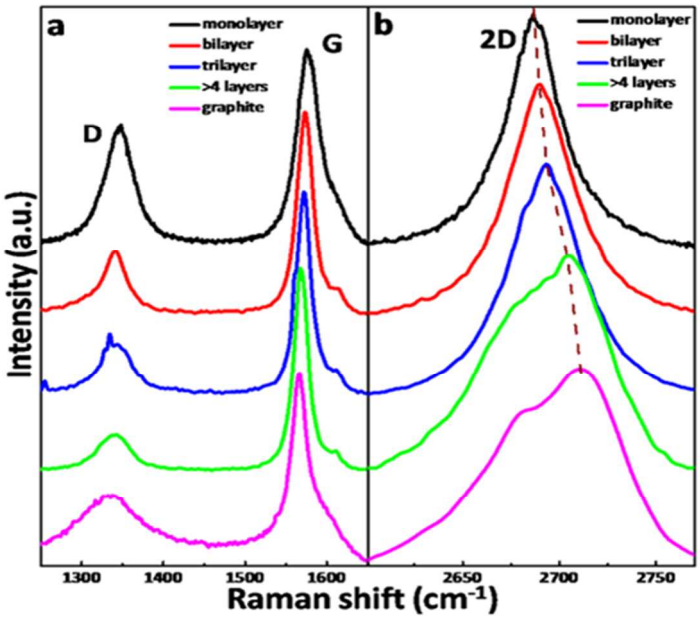

Figure 12. Raman spectra of different layers of graphene. Reprinted with permission from ref. 141.

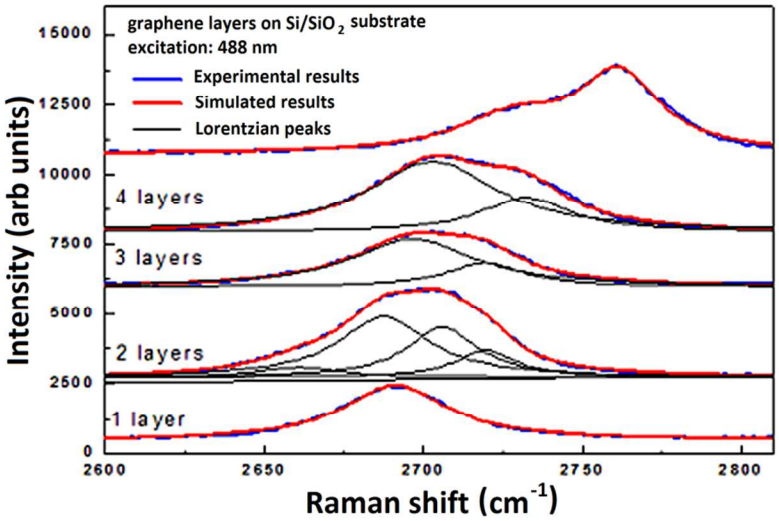

Figure 13. Raman spectrum of 2D band of graphene on Si/SiO_2 substrates as a number of layers changes from one to five. Reprinted with permission from ref. 142.

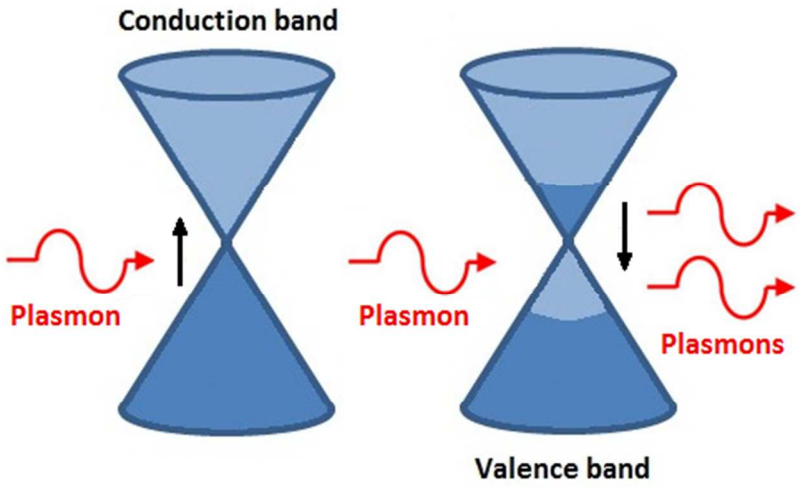

Figure 14. Energy bands of graphene showing stimulated absorption of plasmons (left). Population inverted graphene bands showing stimulated emission of plasmons (Right).

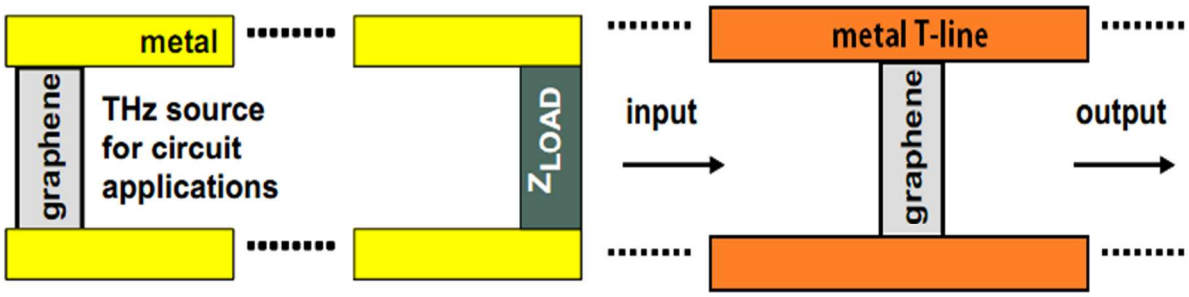

Figure 15. Plasmonic Devices. (a) Illustration of graphene oscillator under load (Left). (b) Illustration of graphene terahertz amplifier. Reprinted with permission from ref. 167.

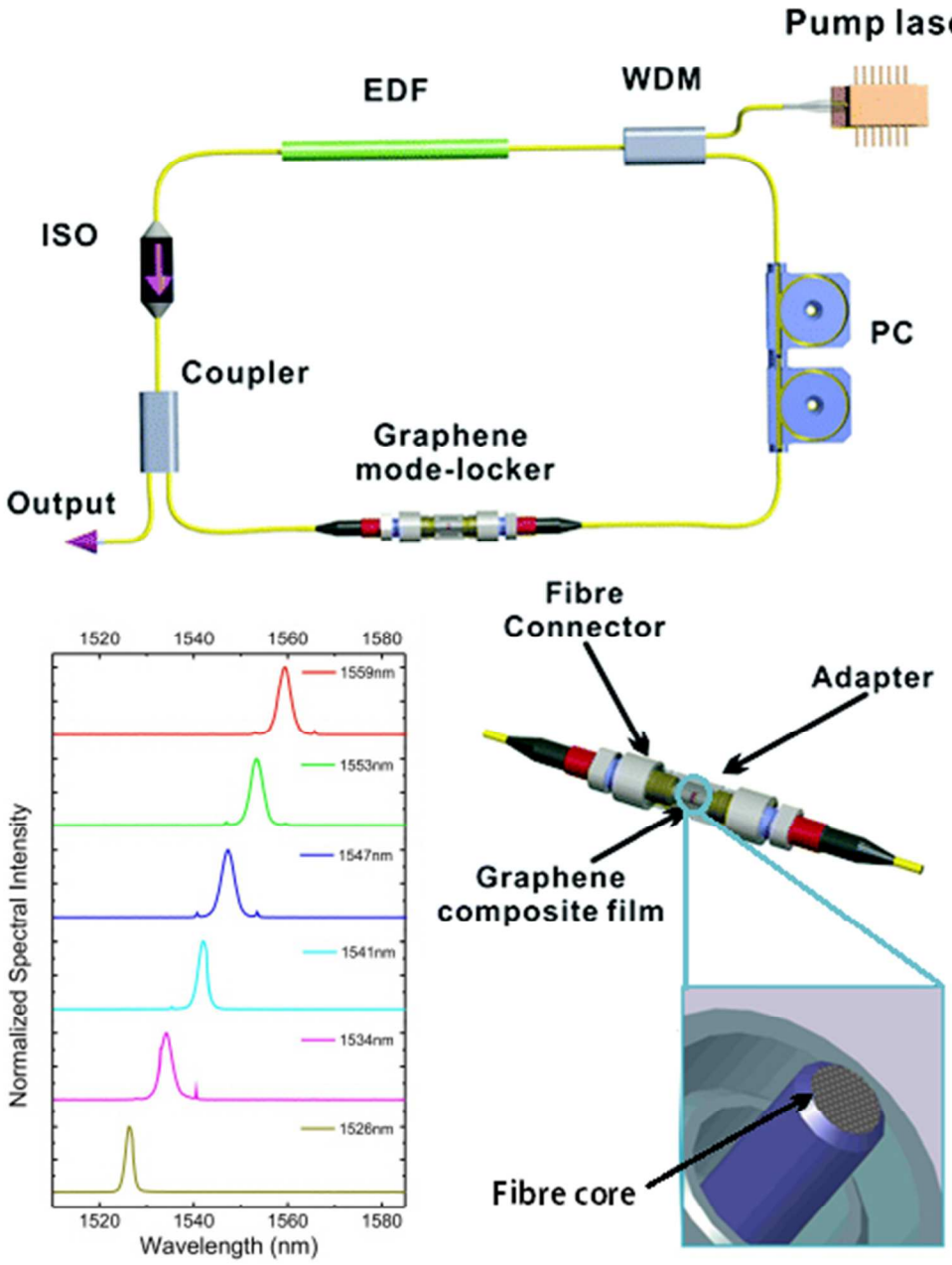

Figure 16. Graphene mode-locked fiber laser and mode-locker assembly. ISO, isolator; WDM, wavelength division multiplexer; PC, polarization controller; EDF, erbium-doped fiber. Reprinted with permission from ref. 174.

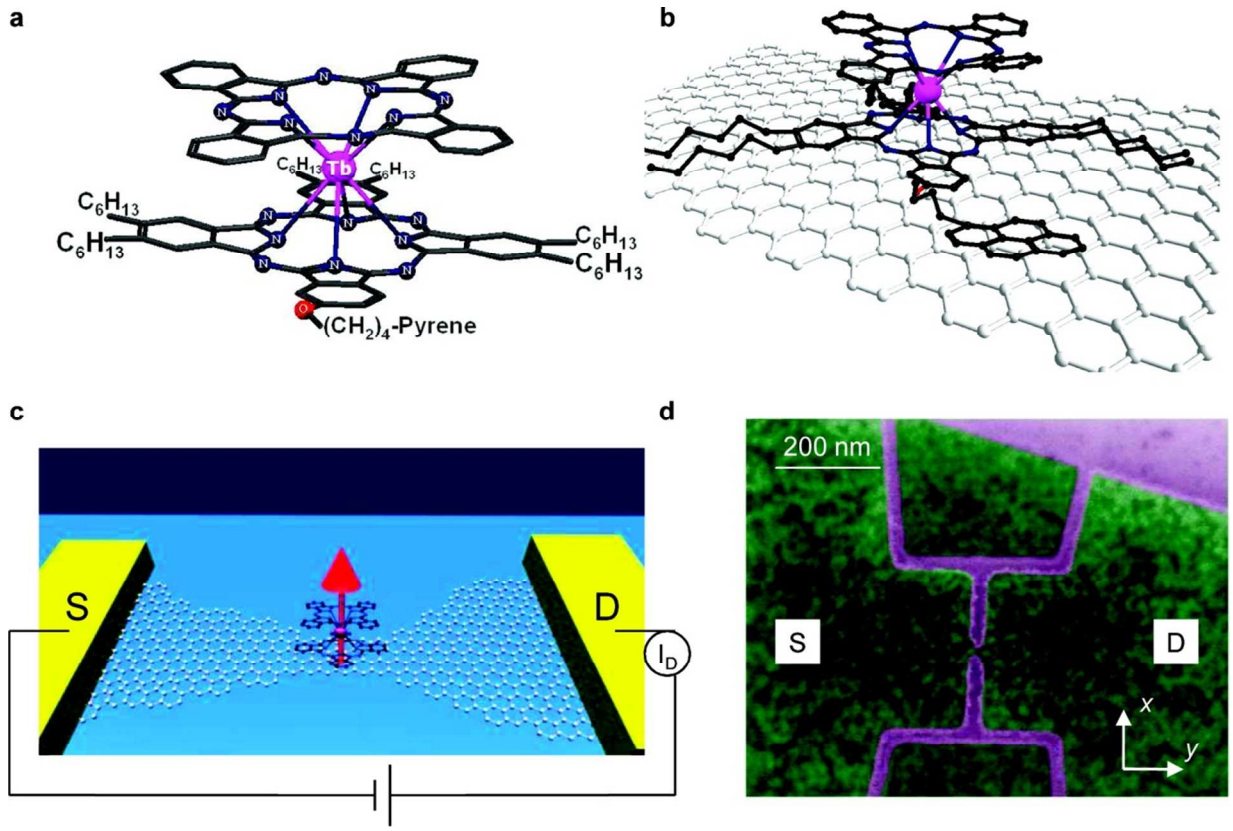

Figure 17. (a) Schematic representation of the $TbPc_2$ single molecule magnet (SMM). (b, c) Schematic view of the device, showing in (b) the molecule attached to graphene and in (c) the nanoconstriction contacted by source (S) and drain (D) electrodes. The magnetic moments of the $TbPc_2$ SMMs (hexyl and pyrenyl groups here omitted for clarity) on top of the constriction add another degree of freedom to tune the conductivity of the device. (d) False-color SEM image of the device presented in the text. SiO_2 substrate and etched graphene are colored in purple. Graphene conductive regions are colored in green. Reprinted with permission from ref. 181.

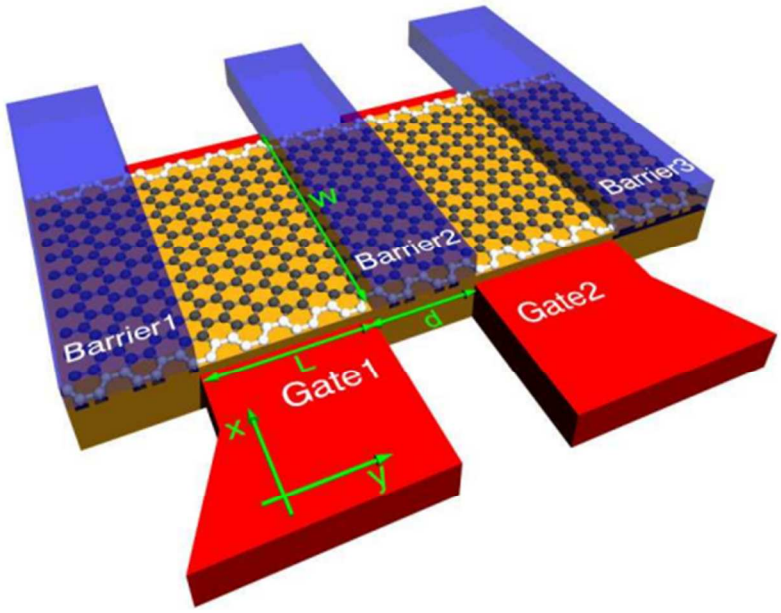

Figure 18. Schematic Illustration of a graphene double quantum dot. Reprinted with permission from ref. 192.

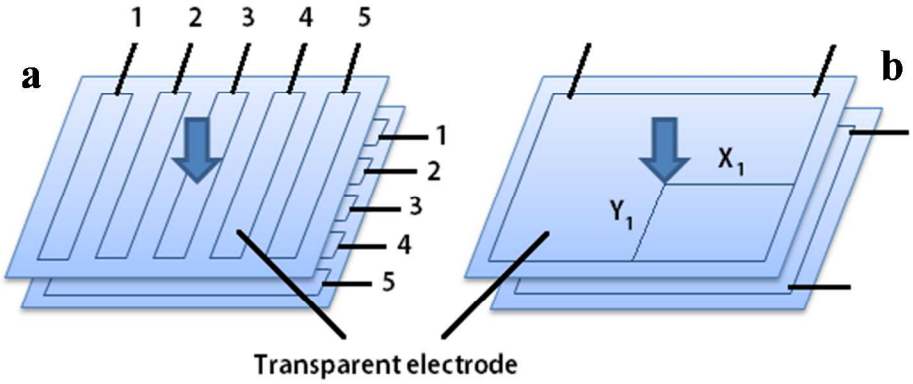

Figure 19. Schematic sketch of the resistive touch panel. (a) matrix-type, (b) analogue-type

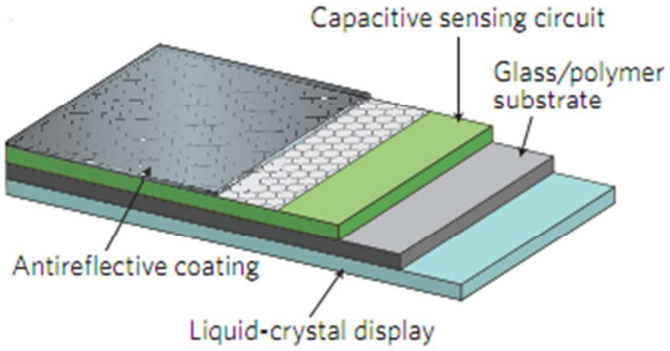

Figure 20. Schematic sketch of the capacitive touch panel. Reprinted with permission from ref. 169.

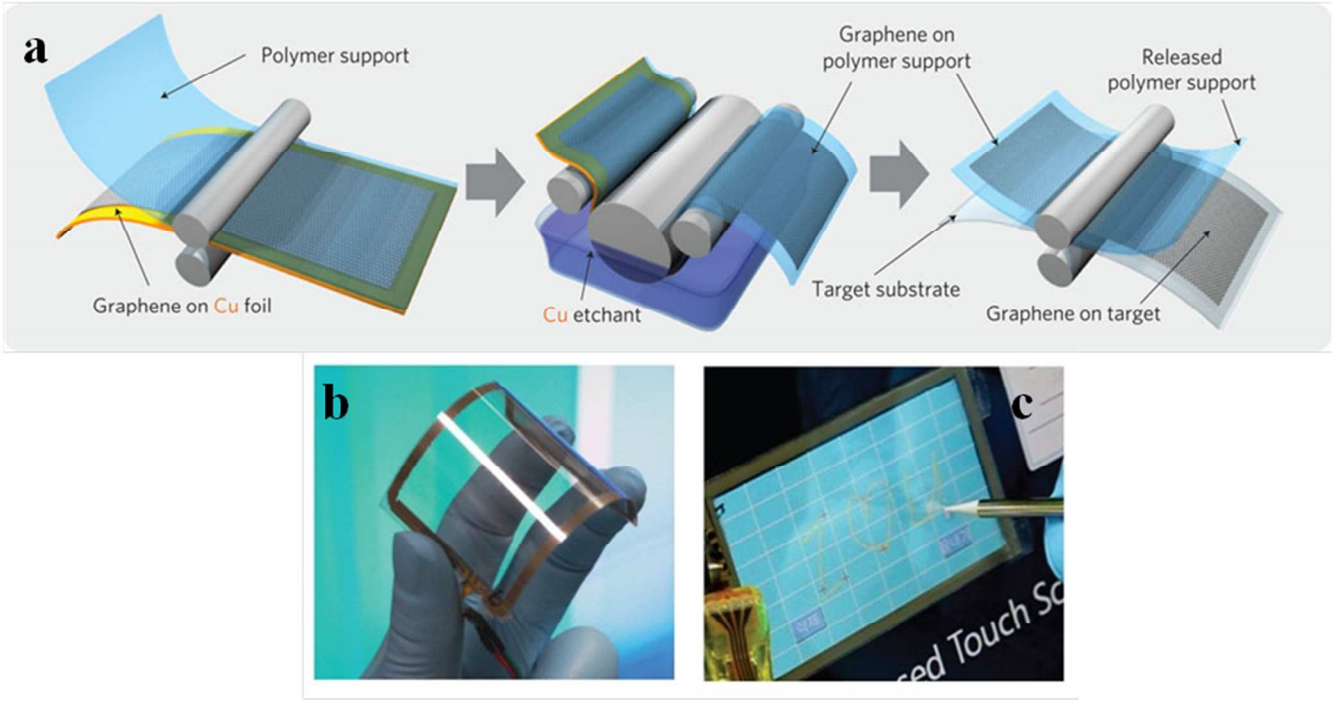

Figure 21. (a). Schematic of the roll-based production of graphene films grown on a copper foil. (b). An assembled graphene/PET touch panel showing outstanding flexibility. (c). A graphene-based touch-screen panel connected to a computer with control software. Reprinted with permission from ref. 194.

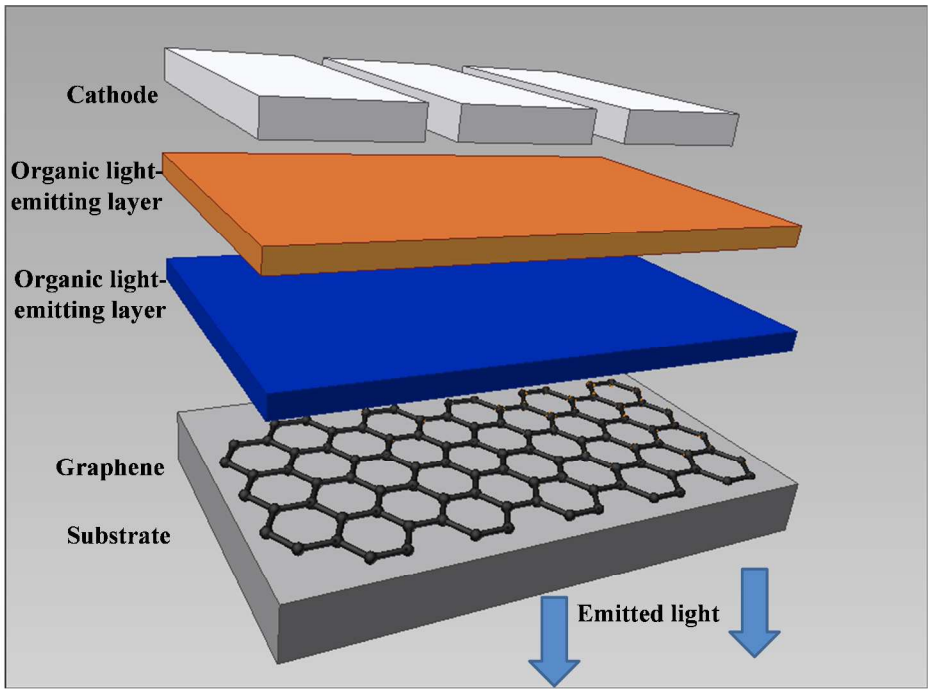

Figure 22. A Schematic of the working mechanism of an Organic Light Emitting Diode.

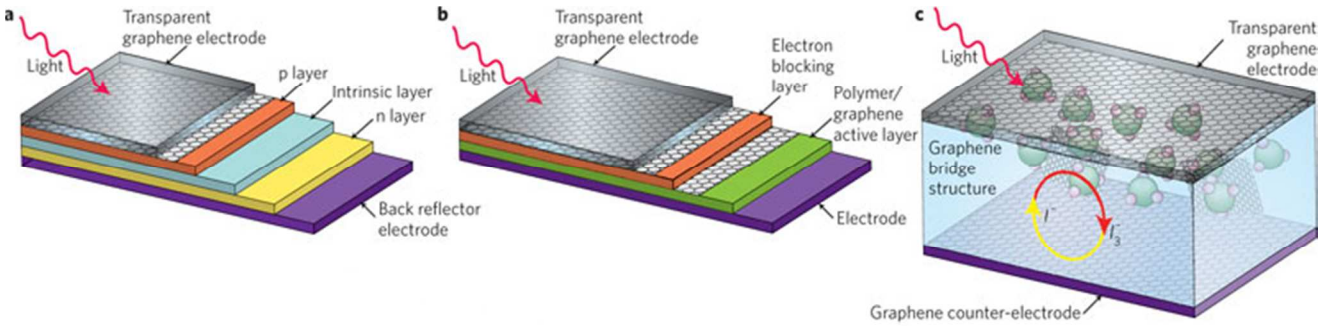

Figure 23. Schematics of inorganic (a), organic (b) and dye-sensitized (c) solar cells. Reprinted with permission from ref. 169.

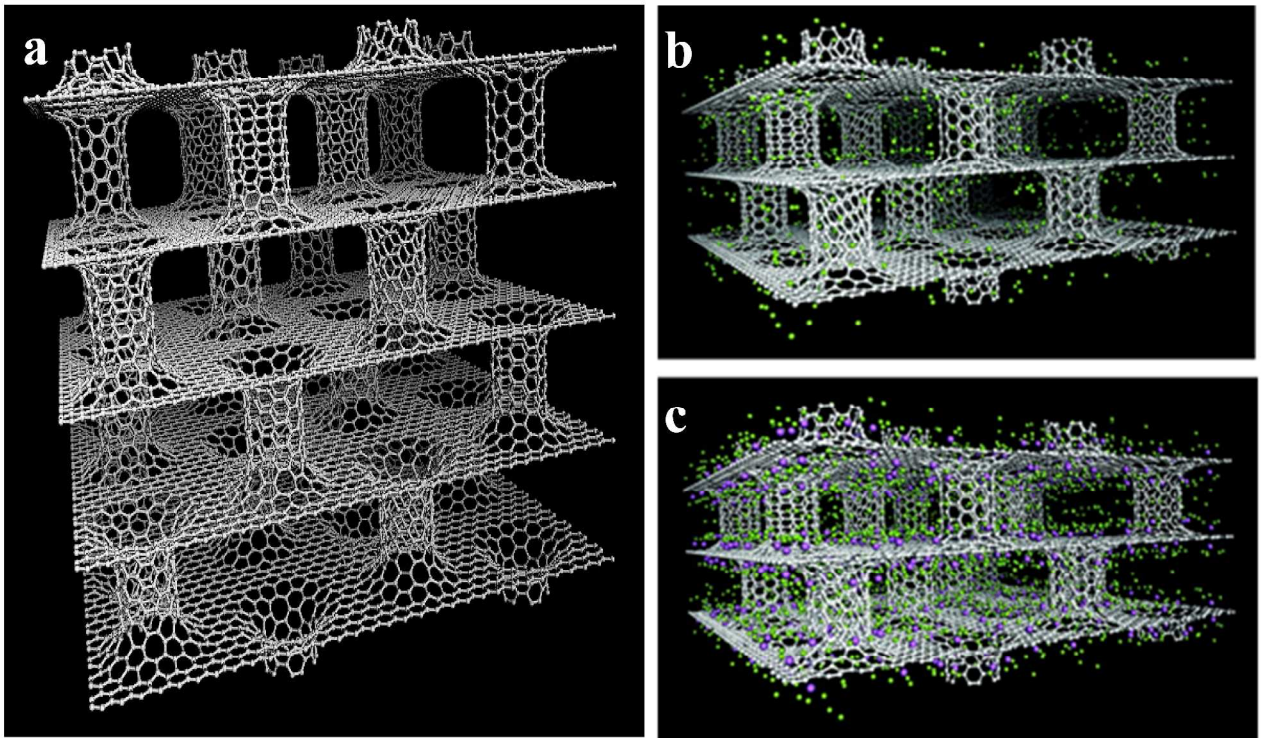

Figure 24. (a). Schematic of Pillared graphene.(b). Snapshot from the GCMC simulations of pure pillared structure at 77 K and 3 bar. Hydrogen molecules are represented in green. (c) Snapshot from the GCMC simulations of lithium doped pillared structure at 77 K and 3 bar. Hydrogen molecules are represented again in green while lithium atoms are in purple. Reprinted with permission from ref. 221.

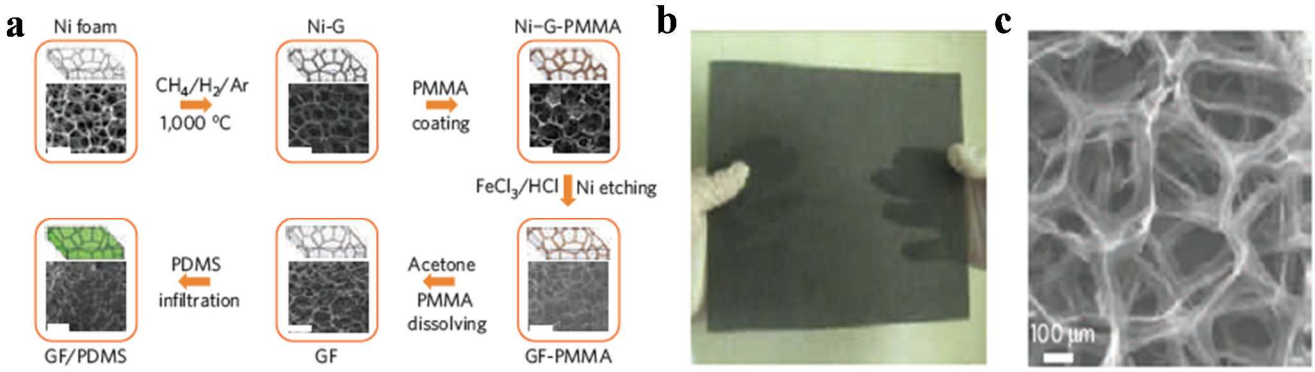

Figure 25. (a) Synthesis of a graphene foam and integration with PDMS. (b) Photograph of a 170 X 220mm^2 free-standing graphene foam.(c) SEM image of a graphene foam. Reprinted with permission from ref. 227.

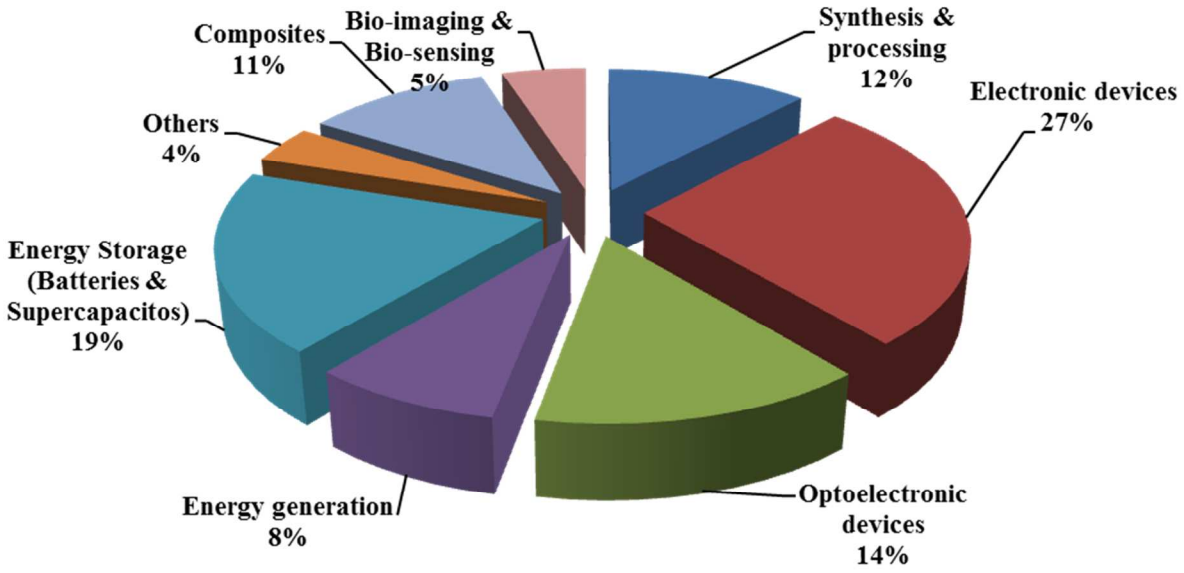

Figure 26. The percentage of various applications of graphene

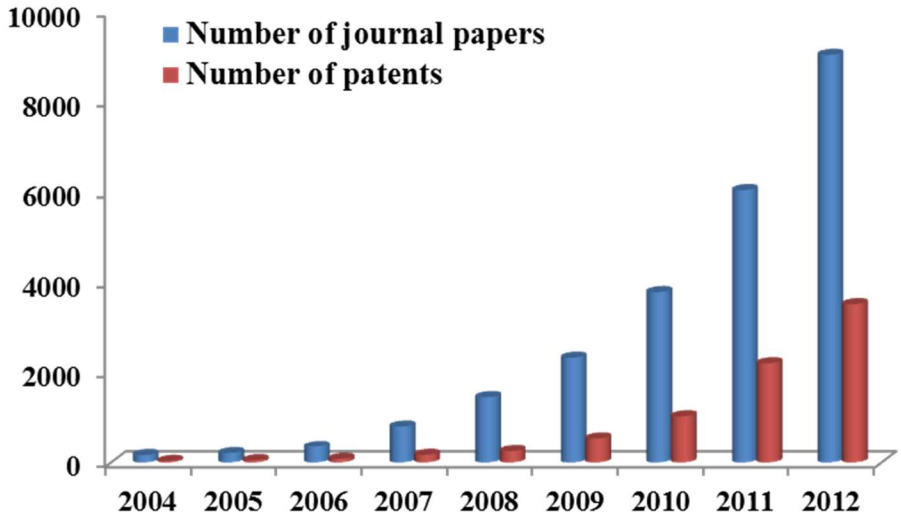

Figure 27. graphene journal papers and patents timeline

Table 1. Properties of Graphene: At a glance

Properties	Graphene	Carbon Nanotubes
Young's Modulus	~ 1 TPa[125]	~ 1 TPa (SWNT)[247] ~ 1.28 TPa (MWNT)[248]
Fracture Strength	130 GPa[125]	~ 30 GPa[247]
Thermal Conductivity	~ 5000 $Wm^{-1}K^{-1}$[137]	~ 2000-7000 $Wm^{-1}K^{-1}$ (SWNT)[249-251] > 3000 $Wm^{-1}K^{-1}$(MWNT)[252]
Thermal Resistance (Interface)	~ 4×10^{-8} K m^2 W^{-1} ($r_{Gr\text{-}SiO2}$)[253]	1.72×10^{-8} K m^2 W^{-1} ($r_{CNT\text{-}SiO2}$)[259]
Specific Surface Area	2630 m^2g^{-1}[215]	15 - 2240 m^2g^{-1}[260, 261]
Optical transmittance	~ 97.7%[103]	~ 90 – 97%[262]
Sheet Resistance	$1.3 \times 10^4 – 5.1 \times 10^4$ Ω/□[103]	200-500 Ω/□[262]
Phase coherence length	3 – 5 μm[254]	150 Å[263]
Spin relaxation length	1.5 – 2 μm[190]	Over tens of μm[264]
Mobility (Typical)	15000 cm^2 V^{-1} s^{-1}[15]	10000 cm^2 V^{-1} s^{-1}[265]
Mobility (Intrinsic)	200,000 cm^2 V^{-1} s^{-1}[255]	100 000 cm^2 V^{-1} s^{-1}[266]
Current Density	10^8 A cm^{-2}[256, 257]	~ 4×10^9 A cm^{-2}[267]
Fermi Velocity	c/300 = 1,000,000 ms^{-1}[258]	8.1×10^5 ms^{-1}[268]
Mean free path (Ballistic electron behaviour)	300-500 nm[258]	0.01-2.2 μm (As produced CNT's), 0.2-13 μm (Purified CNT's)

Table 2. Comparison of CVD processes

Methods	**APCVD**	**LPCVD**	**PECVD**
Temperature (°C)	800 – 1200	500 – 900	600-700
Throughput	High	High	Low
Step coverage	Poor	Conformal	Poor
Film properties	Good	Excellent	Poor

Table 3. Comparison of Fabrication Methods of Graphene

Methods	Mechanism	No. of layers	Precursors used	Nature of graphene obtained	Electronic Quality of layers	Size of layers	Through-put
Mechanical Exfoliation	Peeling layers off using scotch tape	SLG, FLG	Graphite	Pristine	High	10µm	Low
Chemical exfoliation	Decomposition of graphite based compounds, reduction and subsequent exfoliation	SLG, FLG	Graphite Oxide (or) Graphene Oxide obtained by processing GIC's	Chemically Modified Graphene (CMG)	Low	Few 100 nm	High
Liquid phase exfoliation	Exposing graphite or GO to solvents and applying sonification	SLG, FLG	Graphite (or) Graphite Oxide	Pristine	High	Tens of µm to few nm	High
Epitaxial growth	Thermal decomposition of hydrocarbons on top of crystals like SiC, Ru, etc.	SLG, FLG	SiC or Ru	Pristine	High	> 50 µm	Low
Chemical Vapor Deposition	Carbon segregation or precipitation over transition metals	SLG, FLG	Polycrystalline Ni films, copper foils, and other transition metals	Pristine	High	>100 µm (can be in wafer sizes)	Low
Solvo-thermal synthesis	Pyrolysis and filtering of a solvothermal product	SLG, FLG	Solvothermal product (e.g. Na + C_2H_5OH)	CMG	High	Tens of µm to few nm	High
Unzipping Carbon NanoTubes	Longitudinal unzipping of Carbon Nano Tubes	SLG, FLG	Multi-walled carbon nanotubes	CMG	Low	Sub-10 nm	High

Table 4. Advantages and disadvantages of optical microscopy

Advantages	Disadvantages
Relatively simple to use	Limited resolution due to the fixed wavelength of light (400-700nm for visible light)
Rapid identification and characterization of the optical response of thin sheets	Diffraction limits the spatial resolution by nearly half the wavelength of light
Magnifications ranging between 4x to 1000x	Depth of focus decreases with increasing magnification
Non-destructive technique	Requires dielectric coated substrates and optimized parameters for high contrast image

Table 5. Advantages and disadvantages of Scanning Probe Microscopy

Advantages	Disadvantages
Resolution not limited by diffraction, but by the size of probe-sample interaction volume; Generally high resolution	Low throughput and costly and time consuming for examining large area samples
Accurate height measurements at nano scale and resolution at atomic scale – for counting number of layers	Operating platform should be of low vibration and Sample deposition should be done on low roughness surfaces
True 3-D surface maps possible	Small field of view – Requires large quantity of data to make it representative
Can operate in a variety of environments – liquid, vacuum, variable temperature/RH	Images are produced in grayscale, which might exaggerate a specimen's actual shape or size

Table 6. Characterization Techniques: At a glance

Methods		Mechanism	Relative speed	Substrate requirements	Other requirements	Type of Analysis
Optical Microscopy	Interference	Interference contrast	Fast	Dielectrics coated Si	Optimized dielectric thickness and wavelength	Structural
	Ellipsometry	Change in polarization	Fast	Dielectrics coated Si	Optimized dielectric thickness and wavelength	Structural
	Broadband spectro-photometry	Frequency measurement of absorbed light	Fast	Complex substrates (bulk Si & SiO2, Ni, Co, Fe, etc.)	Optimized wavelength range or light incident angle	Structural
	Rayleigh imaging	Elastic light scattering	Fast	Anti-reflection coated dielectric over Si	Monochromatic light/laser, Optimised spacer thickness	Structural
	Fluorescence Quenching Microscopy	Quenching of fluorescent dyes	Fast	Dielectric coated Si	Fluorescein/ PVP coated graphene	Structural
Scanning Probe Microscopy	Scanning Tunnelling Microscopy	Electron tunnelling, Piezo-electric effect	Low scan speed	Conductive, smooth surface	Vacuum	Structural
	Atomic Force Microscopy	Force between sample & tip	Low scan speed	Smooth surface	Vibration-free environment	Structural
Electron Microscopy	Scanning Electron Microscopy	Backscattered / secondary electrons	Medium scan speed	Conductive surface	Vacuum	Structural
	Transmission Electron Microscopy	Transmitted electrons	Slow	Surface transparent to electrons	Vacuum	Structural
	Low Energy	Elastically	Fast as	Conductive	Ultra High	Structural,

	Electron Microscopy	scattered low energy electrons	no rastering needed	surface	Vacuum	elemental
	Low Energy Electron Diffraction	Bombardment with collimated beam of low energy electrons	Slow if accurate results needed	Single crystal substrates	Vacuum	Structural, elemental
	Reflective High Energy Electron Diffraction	Diffraction of high energy electrons	Fast	Single crystal, clean surface	Vacuum	Structural
	Auger Electron Microscopy	Auger electrons	Fast	Conductive / grounded	High vacuum	Elemental
Energy Dispersive X-Ray Analysis (EDX) in SEM		Ejection of e^-,de-excitation	Slow	Conductive / compacted	Moderate vacuum	Elemental
X-Ray Diffraction		Elastic scattering of X-Rays	Fast	Fine powder, randomly distributed	X-Rays	Structural
Spectroscopy Techniques	Raman Spectroscopy	Inelastic photon scattering	Fast	Low fluorescence	Laser	Structural
	Angle resolved Photoemission Spectroscopy	Photoelectric effect	Fast	Clean, atomically flat surfaces	Ultra high vacuum	Structural-Electronic
	X-Ray Photo electron Spectroscopy	Irradiating with a beam of X-Rays	Fast	Flat surface	X-Rays, Ultra high vacuum	Elemental
	UV Photo electron Spectroscopy	Ionizing using UV photons	Rapid	Clean, ordered surface	UV radiation source, Ultra high vacuum	Elemental
	Ion Scattering Spectroscopy	Backscattered ions	Rapid	Conducting surface	Vacuum	Elemental
	Electron Energy Loss Spectroscopy	Scattered inelastic electrons	Fast	Surface transparent to electrons	Thin samples	Elemental

	High-Res Electron Energy Loss Spectroscopy	Scattered inelastic electrons	Slow	Flat, conducting surfaces	Ultra high vacuum	Elemental
	Nuclear Magnetic Resonance Spectroscopy	RF waves at different magnetic field strength	Fast	NMR active materials	RF Waves, Magnetic field	Elemental